Elastohydrodynamic lubrication analysis of a compliant journal bearing considering static and dynamic deformations of the bearing-liner

Mustapha Lahmar, Salah Ellagoune, Benyebka Bou-Saïd

Elastohydrodynamic Lubrication Analysis of a Compliant Journal Bearing Considering Static and Dynamic Deformations of the Bearing Liner

MUSTAPHA LAHMAR[1], SALAH ELLAGOUNE[1], and BENYEBKA BOU-SAÏD[2]
[1]Mechanical Engineering Department, Guelma University
BP 401, Guelma (24000), Algeria
[2]Université de Lyon, CNRS, INSA-Lyon
LaMCoS, UMR5259, F69621, France

In this article, the effect of both static and dynamic deformations of the bearing liner on the dynamic performance characteristics and stability of a water-lubricated, rubber-lined journal bearing operating under small harmonic vibrations is theoretically investigated. To take into account the dynamic deformations of the bearing liner, the first-order perturbation technique is used to determine the eight dynamic coefficients for a given excitation frequency value. The static and dynamic deformation of the fluid/bearing-liner interface is assumed to be proportional to the steady-state and dynamic fluid-film pressures. It was found that the dynamic properties and stability of the compliant finite-length journal bearing are affected by surface coatings from soft materials. It was also shown that when dynamic deformations are considered in the calculations, the dynamic coefficients depend on the excitation frequency, especially for higher values of this parameter. Moreover, the two cross-damping coefficients differ from each other, while the classical elastohydrodynamic (EHD) theory predicts them to be equal, when the dynamic deformations are ignored.

KEY WORDS

EHD Lubrication; Compliant Journal Bearings; Static Deformation; Dynamic Deformation; Stiffness And Damping Coefficients; Stability; Perturbation Technique; Compressible Thin Elastic Liner Model

INTRODUCTION

The compliant plain journal bearings are the machine elements that consist of two components: a shaft in hard steel and a bearing with a liner. Technologically speaking, the coated bearings are used in order to reduce the friction coefficient in the boundary lubrication regime encountered mainly during the start and stop phases of machines.

Since 1965, steady-state performance characteristics of compliant journal bearings have theoretically and experimentally been investigated by many researchers *(1-16)*. However, dynamic properties have mostly been calculated by taking into consideration only static-pressure–induced deformations of the bearing liner—even for low-elasticity modulus materials such as white metals and rubber materials. Indeed, the existing literature shows that studies on dynamic characteristics of compliant journal bearings considering dynamic-pressure–induced deformations of the bearing liner are scarce.

A good survey on EHD investigations in both static and dynamic operating conditions of steadily and dynamically loaded compliant journal bearings can be found in References *(11, 12, 14)*.

An example of a compliant journal bearing is the water-lubricated rubber journal bearing that is used in many applications, including stern tube bearings on ships, submarines, and hydraulic pumps.

The rubber journal bearings reduce much noise and vibration (acoustic emissions) compared with equivalent composite bearings. These bearings are resistant to abrasion caused by the presence of solid particles in the water. The use of water as a lubricant provides efficient low-friction operation and a stable lubricant film due to the water's incompressibility.

Figure 1 shows a picture of a typical water-lubricated propeller shaft bearing system. To promote the formation of a hydrodynamic film between the propeller shaft and bearing, the lower loaded half of the bearing is smooth, while the upper one incorporates longitudinal grooves for flow of the water lubricant. The rigid outer shell is made of naval brass or nonmetallic composite, which acts as the compliant liner rigid backing.

The first designs of these bearings had a plain bore, but this was modified several times in order to improve the performance characteristics of the bearing.

There is another generation of marine bearings like straight-fluted bearings widely used today. The design of this type of bearings consists of a number of rubber staves (load-carrying lands) bonded onto the outer rigid shell and separated by flutes. These flutes supply the bearing with water lubricant that enters at one end of the bearing and leaves at the other one.

NOMENCLATURE

$a_{\varepsilon\varepsilon}, a_{\varepsilon\phi}, a_{\phi\varepsilon}, a_{\phi\phi}$ = stiffness coefficients, N/m

$A_{\varepsilon\varepsilon}$, $A_{\varepsilon\phi}, A_{\phi\varepsilon}$, $A_{\phi\phi}$ = dimensionless stiffness coefficients, $A_{ij} = a_{ij}\frac{C^3}{\mu\omega R^3 L}$; $(i,j) = (\varepsilon, \phi)$

$b_{\varepsilon\varepsilon}$, $b_{\varepsilon\phi}, b_{\phi\varepsilon}, b_{\phi\phi}$ = damping coefficients, $N.s/m$

$B_{\varepsilon\varepsilon}$, $B_{\varepsilon\phi}, B_{\phi\varepsilon}, B_{\phi\phi}$ = dimensionless damping coefficients, $B_{ij} = b_{ij}\frac{C^3}{\mu R^3 L}$; $(i,j) = (\varepsilon, \phi)$

C = bearing radial clearance, m

$\tilde{C}_d$ = deformation coefficient, $\tilde{C}_d = \frac{\mu\omega(R/C)^3}{E}$

E = Young's modulus of the bearing-liner material, Pa

e = eccentricity, m

e_0 = steady-state eccentricity, $e_0 = \overline{|O_b O_{j0}|}$, m

F_{ε_0}, F_{ϕ_0} = steady-state hydrodynamic force components, N

g = gravitational acceleration, ms^{-2}

h = fluid-film thickness, m

$\tilde{h}$ = dimensionless fluid-film thickness, $\tilde{h} = \frac{h}{C}$

h_0 = static fluid-film thickness, m

$\tilde{h}_0$ = dimensionless static fluid-film thickness, $\tilde{h}_0 = \frac{h_0}{C}$

$\tilde{h}_{0_{\min}}$ = minimum static film thickness

L = length of bearing, m

L_0 = scalar compliance operator

$\tilde{L}_0$ = dimensionless compliance operator

M = mass of rotor per bearing, kg

$\tilde{M}$ = dimensionless mass, $\tilde{M} = \frac{MC\omega^2}{W_0}$

M_c = critical mass of the rotor-bearing system, kg

$\tilde{M}_c$ = dimensionless critical mass (stability parameter), $\tilde{M}_c = \frac{M_c^C \omega^2}{W_0}$

n = rotation velocity of the journal, rpm

p = fluid-film pressure, Pa

$\tilde{p}$ = normalized film pressure, $\tilde{p} = \frac{p}{\mu_0^{\omega}(\frac{R}{C})^2}$

p_0 = static pressure, Pa

$\tilde{p}_0$ = normalized static pressure, $\tilde{p}_0 = \frac{p_0}{\mu_0^{\omega}\left(\frac{R}{C}\right)^2}$

$\tilde{p}_{0_{\max}}$ = maximum static film pressure

$\tilde{Q}$ = complex amplitude of the dimensionless dynamic pressure

$\tilde{Q}_\varepsilon, \tilde{Q}_\phi$ = normalized dynamic pressures, $(\tilde{Q}_\varepsilon, \tilde{Q}_\phi) = \left(\frac{\partial\tilde{Q}}{\partial\varepsilon}, \frac{1}{\varepsilon_0}\frac{\partial\tilde{Q}}{\partial\phi}\right)$

R = journal radius, m

S = Sommerfeld number, $S = \frac{\mu\omega RL(R/C)^2}{\pi W_0}$

t = time, s

$\tilde{t}$ = dimensionless time, $\tilde{t} = \omega t$

t_h = thickness of the bearing liner, m

$\tilde{t}_h$ = relative thickness of the bearing liner, $\tilde{t}_h = {}^{t_h}/_{R}$

$\tilde{U}$ = complex amplitude of the dimensionless dynamic deformation

U_0 = static deformation of the bearing liner, m

$\tilde{U}_0$ = dimensionless static deformation, $\tilde{U}_0 = \frac{U_0}{C}$

$\tilde{U}_\varepsilon, \tilde{U}_\phi$ = normalized dynamic deformations of the bearing liner, $(\tilde{U}_\varepsilon, \tilde{U}_\phi) = \left(\frac{\partial\tilde{U}}{\partial\varepsilon}, \frac{1}{\varepsilon_0}\frac{\partial\tilde{U}}{\partial\phi}\right)$

W_0 = static load applied on the journal bearing, $W_0 = Mg$, N

$X, Y =$ = displacement components of the journal center, m

$\tilde{X}, \tilde{Y}$ = dimensionless displacements, $(\tilde{X}, \tilde{Y}) = \frac{(X,Y)}{C}$

z = axial coordinate measured from middle section plane of the bearing, m

$\tilde{z}$ = nondimensional axial coordinate, $\tilde{z} = \frac{z}{L}$

ε = eccentricity ratio, $\varepsilon = \frac{e}{C}$

ε_0 = steady-state eccentricity ratio, $\varepsilon_0 = \frac{e_0}{C}$

ϕ = bearing attitude angle, rad

ϕ_0 = steady-state attitude angle, $\phi_0 = Tan^{-1}\left(-\frac{F_{\phi_0}}{F_{\varepsilon_0}}\right)$

γ = excitation frequency ratio, $\gamma = \frac{\nu}{\omega}$

γ_c = whirl frequency ratio (stability parameter), $\gamma_c = \frac{\nu_c}{\omega}$

μ = absolute viscosity of lubricating fluid, $Pa.s$

G = shear modulus of the bearing-liner material, Pa

σ = Poisson's ratio of the bearing-liner material

ν = excitation frequency, rad/s

θ = bearing angle with the origin situated at the maximum film thickness, rad

θ_{c_0} = static cavitation angle, rad

ω = angular velocity of the journal, $\omega = 2\pi n/60$, rad/s

$\dot{(\bullet)}$ = denotes differentiation with respect to t

$(\bullet)'$ = denotes differentiation with respect to $\tilde{t}$, $(\bullet)' = \frac{1}{\omega}(\dot{\bullet})$

$[\bullet]$ = square matrix

$(\bullet)^T$ = transpose of $(\bullet)$

$\sim$ = on top of a variable denotes a dimensionless quantity

Frames

$(O_b X, Y, Z)$ = stationary rectangular coordinate system with origin at the bearing geometric center

(x, y, z) = local coordinate system of the journal bearing

(O_b, ε, ϕ) = rotating rectangular coordinate system with origin at the bearing geometric center

Abbreviations

EHD = Elasto-Hydro-Dynamic

JFO = Jakobsson Floberg Olsson

Im( ) = Imaginary part of ( )

Real( ) = Real part of ( )

Certain marine bearings are made from molded rubber staves that, when assembled, form an uninterrupted cylindrical bore bounded by a hard backing metal. The steady-state performance characteristics of this type of bearings have been investigated extensively by several researchers, including Braun and Dougherty *(11, 12)*. They have found that the liner compliance strongly affects the maximum steady-state pressure and the cavitation zone location, especially at high values of eccentricity and angular velocity.

In the present investigation, the governing equations relative to this situation are established, and a numerical simulation is performed. We analyzed the effects of both static and dynamic deformations of the bearing liner on the stiffness and damping coefficients, critical mass, and whirl frequency of a finite-length water-lubricated rubber-lined journal bearing operating under small harmonic vibrations.

The first-order perturbation technique was used to determine static and complex dynamic pressures developed in the fluid film.

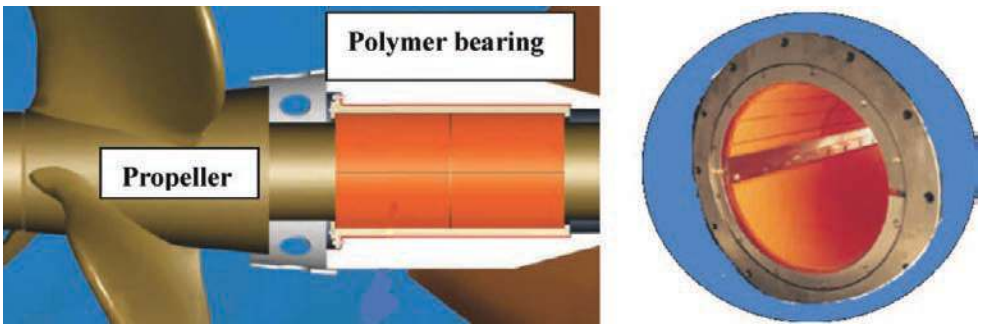

Fig. 1—View of a typical water-lubricated propeller shaft bearing system.

The eight dynamic coefficients can be obtained by means of numerical integrations for a given excitation frequency value. The dynamic coefficients were used as input data for studying the linear stability of the rotor-bearing system.

As a first approximation, the deformations of the thin elastic liner made from either compressible or almost incompressible materials were assumed to be proportional to the fluid-film pressures. The calculations were generally performed for the following cases:

1. rigid bearing liner;
2. only static deformation;
3. both static and dynamic deformations.

THEORETICAL ANALYSIS

Figure 2 schematically shows the aligned compliant plain journal bearing at its static equilibrium position with an elastically deformed bearing liner where the undeformed (rigid) configuration is represented by the circle of radius $(R + C)$. The origin of the stationary X, Y, Z coordinate system is located at the center of the rigid bearing O_b. The circumferential coordinate θ is measured from the negative ε axis (line of centers). The journal with radius R is assumed to be rigid and rotates with a constant angular velocity ω about the Z axis. The static position of its geometric center is defined by the steady-state eccentricity $e_0 = C\varepsilon_0$ and the steady-state attitude angle ϕ_0. The radial clearance when the journal and bearing circles are concentric of the rigid bearing is given by C, and the steady-state film thickness including the static radial deformation of the bearing liner U_0 is measured by h_0. The steady-state film thickness can be found using the cosine rule of triangle $(O_b - O_{j_0} - M)$:

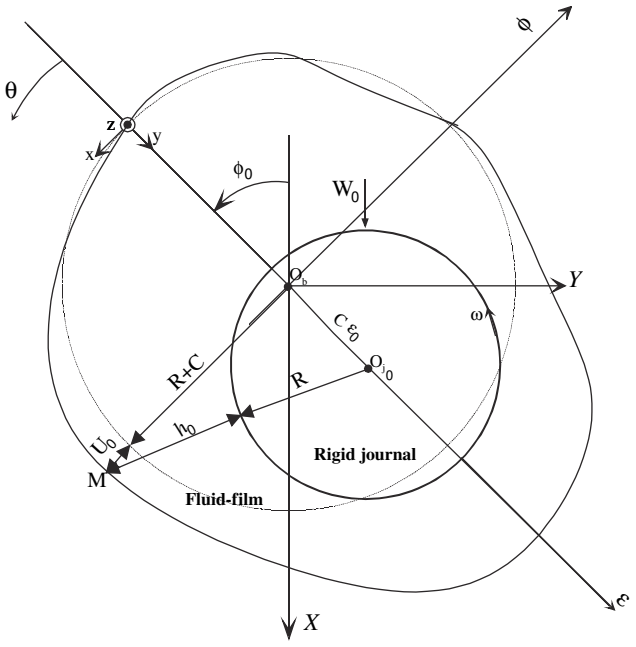

Fig. 2—Geometry of a compliant plain journal bearing.

$$(R + h_0)^2 = (R + C + U_0)^2 + e_0^2 + 2\,(R + C + U_0)\, e_0 \cos\theta \quad [1]$$

Expanding this equation, dividing by R^2, and neglecting second-order terms in h_0/R, C/R, e_0/R , and U_0/R yields

$$h_0 = C\,(1 + \varepsilon_0 \cos\theta) + U_0, \quad [2]$$

where

$$U_0 = \frac{(\chi - 1)}{(\chi + 1)} \frac{t_h}{G} p_0. \quad [3]$$

In Eq. [3], t_h is the thickness of the bearing liner, p_0 is the steady-state hydrodynamic pressure,

$$G = \frac{E}{2\,(1 + \sigma)}$$

is the shear modulus known as the Coulomb's elasticity modulus, and χ is the elasticity parameter depending on the Poisson's ratio σ ($\chi = 3 - 4\sigma$ for the plane strain elasticity problem, and $\chi = \frac{3-\sigma}{1+\sigma}$ for the plane stress problem).

Assuming plane strain (i.e., $\chi = 3 - 4\sigma$) and compressible materials case ($\sigma < 1/2$), the radial deformation field of a thin elastic liner fixed on a rigid backing can be calculated with a sufficient accuracy by

$$U_0 = \sigma_0 \frac{t_h}{E} p_0, \quad [4a]$$

where $\sigma_0 = \frac{(1+\sigma)(1-2\sigma)}{1-\sigma}$, and E and σ are the Young's modulus and the Poisson's ratio of the bearing liner, respectively. Eq. [4a] can be rewritten as

$$U_0 = L_0 p_0, \quad [4b]$$

where $L_0 = \sigma_0 \frac{t_h}{E}$ is a scalar compliance operator.

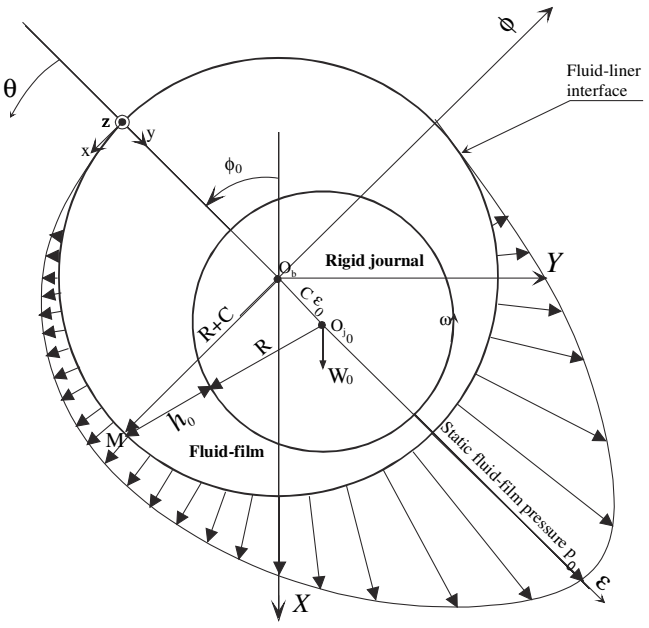

Fig. 3—Geometry of a rigid plain journal bearing.

Note that Eq. [4a] is obtained from Eq. [3] by replacing the elasticity parameter χ and the shear modulus G with their expressions.

For the rigid bearing liner (Fig. 3), Eq. [2] reduces to

$$h_0 = C(1 + \varepsilon_0 \cos\theta). \qquad [5]$$

The simplified compressible thin elastic liner model (Eq. [4]) has been successfully applied by several investigators for EHD analyses of single-layered journal bearings *(5, 6)*. Compared to the finite element method, the main advantage of this model is its low cost of space memory and CPU-time consumption as well as its easy implementation. However, the thin elastic liner model ceases to be valid when the bearing-liner Poisson's ratio becomes greater than 0.4, i.e., for almost incompressible materials, and in the case of thick liners. (See References *(14, 16)* for the detailed demonstrations about the derivation and the validation of thin elastic liner model.)

For isoviscous and isovolume lubricants such as water, the pressure field under isothermal laminar flow condition in the clearance space of the journal bearing (Fig. 2) must satisfy the unsteady-state Newtonian Reynolds' equation (Eq. [17]):

$$\frac{1}{R^2}\frac{\partial}{\partial\theta}\left(\frac{h^3}{12}\frac{\partial p}{\partial\theta}\right) + \frac{\partial}{\partial z}\left(\frac{h^3}{12}\frac{\partial p}{\partial z}\right) = \frac{1}{2}\mu\omega\frac{\partial h}{\partial\theta} + \mu\frac{\partial h}{\partial t} \qquad [6]$$

or its dimensionless form

$$\frac{\partial}{\partial\theta}\left(\frac{\tilde{h}^3}{12}\frac{\partial\tilde{p}}{\partial\theta}\right) + (R/L)^2\frac{\partial}{\partial\tilde{z}}\left(\frac{\tilde{h}^3}{12}\frac{\partial\tilde{p}}{\partial\tilde{z}}\right) = \frac{1}{2}\frac{\partial\tilde{h}}{\partial\theta} + \frac{\partial\tilde{h}}{\partial\tilde{t}}, \qquad [7]$$

where $\tilde{h} = \frac{h}{C}$, $\tilde{p} = \frac{p}{\mu\omega(R/C)^2}$, $\tilde{z} = \frac{z}{L}$, and $\tilde{t} = \omega t$.

The above assumptions used on the lubricating fluid and its flow in the thin gap between the journal and the bearing are appropriate for low-viscosity lubricants such as water, producing a small amount of dissipation energy and leading to negligible variations of the viscosity with respect to pressure and temperature. Indeed, the thermal and piezoviscous effects are more significant in the case of very viscous fluids such as oils used in rolling bearings and gears applications that operate at very high pressures.

As we suppose a pinching lubrication process, the hydrodynamic pressure $\tilde{p}\,(\theta, \tilde{z}, \tilde{t})$ must satisfy the following boundary conditions:

(1) on the bearing sides,

$$\tilde{p}(\theta, \tilde{z} = -1/2, \tilde{t}) = \tilde{p}(\theta, \tilde{z} = 1/2, \tilde{t}) = 0; \qquad [8]$$

(2) the pressure is continuous and periodic in the circumferential direction, i. e.,

$$\tilde{p}(\theta, \tilde{z}, \tilde{t}) = \tilde{p}(\theta + 2\pi, \tilde{z}, \tilde{t}); \qquad [9]$$

(3) at the leading edge of the cavitation zone $\theta = \theta_c\,(\tilde{z})$, the pressure and its gradients vanish, i.e.,

$$\tilde{p} = \frac{\partial\tilde{p}}{\partial\theta} = \frac{\partial\tilde{p}}{\partial\tilde{z}} = 0. \qquad [10]$$

These conditions, which were suggested in the early 1930s and known as the Reynolds or Swift-Stieber cavitation conditions *(18, 19)*, can be satisfied in a direct manner if the Christopherson's algorithm *(20)* is employed. This algorithm has been successfully used for very long time (since the 1940s) in the simulation studies of lubrication problems. However, the use of Christopherson's algorithm leads to the determination of an erroneous boundary of film reformation (trailing edge of the cavitation zone). The mass flow continuity is not fulfilled. It should be noted that the Reynolds boundary conditions [10] are very frequently used, giving results comparable to those obtained experimentally or by using the conservation algorithms such as the JFO, Elrod-Adams, and Bayada cavitation models, with the exception of the value of the rate of flow *(21-23)*.

In References *(23)*, Dowson and Taylor presented an excellent review of cavitation phenomenon in the hydrodynamic journal bearings, where different cavitation models were largely discussed.

If the journal is excited into a simple harmonic motion of small amplitudes within the compliant bearing at frequency ν, the instantaneous eccentricity ratio and attitude angle may be expressed respectively as

$$\varepsilon = \varepsilon_0 + \Delta\varepsilon\, e^{i\gamma\tilde{t}} \text{ and } \phi = \phi_0 + \Delta\phi\, e^{i\gamma\tilde{t}};$$
$$|\Delta\varepsilon| \ll \varepsilon_0\,, |\Delta\phi| \ll \phi_0 \text{ and } i = \sqrt{-1}, \qquad [11]$$

where $\gamma = \nu/\omega$ is the relative excitation frequency, and $\Delta\varepsilon$ and $\Delta\phi$ are complex amplitudes of eccentricity ratio and attitude angle, respectively. The corresponding dynamic increment of dimensionless film thickness may be expressed as *(24)*

$$\tilde{h} = \tilde{h}_0 + \tilde{h}_d + \tilde{U}_d, \qquad [12]$$

where $\tilde{h}_0 = \frac{h_0}{C}$ is the dimensionless steady-state film thickness including the steady-state deformation of the bearing-liner

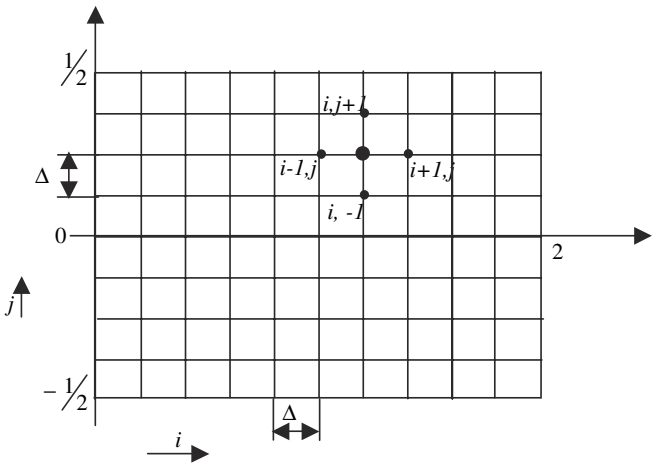

Fig. 4—Finite difference grid for the solution of the static and dynamic Reynolds' equations.

(Eq. [2]), $\tilde{h}_d = (\Delta\varepsilon\,\cos\theta + \varepsilon_0\Delta\phi\,\sin\theta)\,e^{i\gamma\tilde{t}}$ is the change in fluid-film thickness due to dynamic movement of the journal, and $\tilde{U}_d = \tilde{U}e^{i\gamma\tilde{t}} = \left(\Delta\varepsilon\,\tilde{U}_\varepsilon + \varepsilon_0\Delta\phi\,\tilde{U}_\phi\right)\,e^{i\gamma\tilde{t}}$ is the dynamic deformation caused by the dynamic increment of film pressure where

$$\tilde{U}_\varepsilon = \frac{\partial\tilde{U}}{\partial\varepsilon},\ \tilde{U}_\phi = \frac{1}{\varepsilon_0}\frac{\partial\tilde{U}}{\partial\phi},$$

and $\tilde{U}$ is the complex amplitude.

Of course we suppose here that we are in the case of the application of the principle of superposition. As we assume that we are in small harmonic motion amplitudes and for the deformation in linear situation, we can consider this hypothesis reasonable if we add the additional terms to $\tilde{h}_0$, i.e., $\tilde{h}_d + \tilde{U}_d$ is small compared to $\tilde{h}_0$. Of course with the help of nonlinear modelling, one can more precisely give the significance of small and its limits.

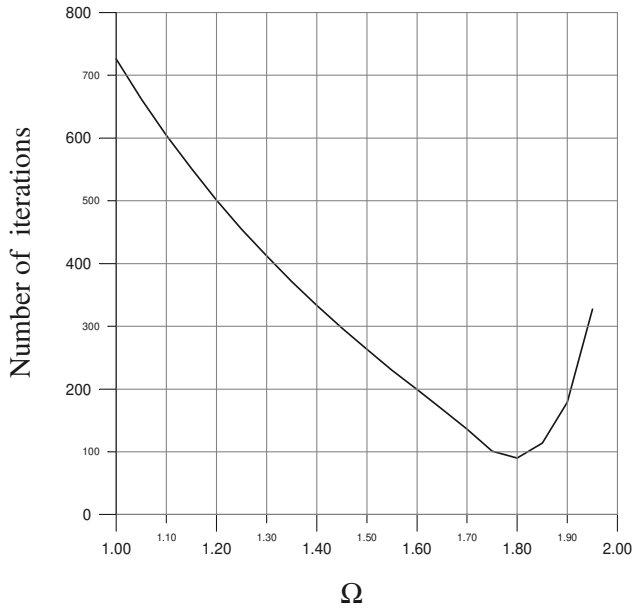

Fig. 5—Determination of the optimum value of the over-relaxation factor.

Consequently, the instantaneous value of dimensionless film thickness may be expressed as

$$\tilde{h} = \tilde{h}_0 + (\Delta\varepsilon(\cos\theta + \tilde{U}_\varepsilon) + \varepsilon_0\Delta\phi(\sin\theta + \tilde{U}_\phi))\,e^{i\gamma\tilde{t}}. \qquad [13]$$

The first and second terms on the RHS of Eq. [13] correspond to the steady-state and dynamic components, respectively.

The instantaneous value of the dimensionless resultant film pressure is then expressed as

$$\tilde{p} = \tilde{p}_0 + \tilde{Q}\,e^{i\gamma\tilde{t}}, \qquad [14]$$

where $\tilde{p}_0$ is the dimensionless steady-state pressure, and $\tilde{Q} = \Delta\varepsilon\ \tilde{Q}_\varepsilon + \varepsilon_0\Delta\phi\ \tilde{Q}_\phi$ is the complex dynamic increment of the film pressure, where $\tilde{Q}_\varepsilon = \frac{\partial\tilde{Q}}{\partial\varepsilon}$ and $\tilde{Q}_\phi = \frac{1}{\varepsilon_0}\frac{\partial\tilde{Q}}{\partial\phi}$.

Note that adding the dynamic deformations $\tilde{U}_\varepsilon$ and $\tilde{U}_\phi$ in Eq. [13] gives a more complete expression of the film thickness than if only static deformation is taken into consideration.

The dynamic deformations are also calculated using the thin elastic liner model, i.e.,

$$\tilde{U}_\varepsilon = \tilde{L}_0\,\tilde{Q}_\varepsilon \text{ and } \tilde{U}_\phi = \tilde{L}_0\,\tilde{Q}_\phi, \qquad [15]$$

where

$$\tilde{L}_0 = \sigma_0\,\tilde{C}_d\,\tilde{t}_h. \qquad [16]$$

In Eq. [16], $\tilde{C}_d = \frac{\mu\omega(R/C)^3}{E}$ is the dimensionless deformation coefficient varying from 0 to ∞, and $\tilde{t}_h = t_h/R$ is the relative thickness of the bearing liner.

TABLE 1—COMPARISON OF STEADY-STATE AND DYNAMIC PERFORMANCE CHARACTERISTICS FOR A RIGID FINITE-LENGTH PLAIN JOURNAL BEARING ($\frac{R}{L} = 0,5$)

ε_0	0.0962	0.5374	0.8349	Note
S	**1.03540**	**0.1549**	**0.0345**	(1)
	1.03610	0.1559	0.0350	(2)
ϕ_0(deg)	**84.03**	**56.07**	**33.03**	(1)
	84.07	56.22	33.59	(2)
A_{XX}	**1.004**	**2.154**	**6.585**	(1)
	1.100	2.140	6.467	(2)
A_{XY}	**10.630**	**3.181**	**4.302**	(1)
	10.613	3.182	4.237	(2)
A_{YX}	**–10.250**	**–0.886**	**0.837**	(1)
	–10.233	–0.887	0.757	(2)
A_{YY}	**2.157**	**2.002**	**1.961**	(1)
	2.144	1.994	1.901	(2)
B_{XX}	**21.149**	**5.867**	**7.383**	(1)
	21.133	5.874	7.434	(2)
B_{YX}	**2.112**	**2.093**	**2.020**	(1)
	2.147	2.085	2.061	(2)
B_{YY}	**20.703**	**3.110**	**1.314**	(1)
	20.694	3.117	1.372	(2)
$\bar{M}_c$	**6.416**	**6.757**	**Stable position**	(1)
	6.422	6.757	"	(2)
γ_c	**0.501**	**0.474**	**Stable position**	(1)
	0.500	0.473	"	(2)

[1]Published results from Reference *(27)*.
[2]Present work.

TABLE 2—GEOMETRIC CHARACTERISTICS AND OPERATING CONDITIONS OF THE COMPLIANT JOURNAL BEARING ($\frac{R}{L} = 0, 5$)

Parameter	Symbol	Unit	Value
Bearing length	L	m	0.050
Journal radius	R	m	0.025
Radial clearance	C	m	50×10^{-6}
Thickness of the bearing liner	t_h	m	0.010
Dynamic viscosity of lubricant (water at 20°C)	μ	$Pa.s$	0.001
Angular velocity of the journal	ω	$rad.s^{-1}$	$100 \times \pi$
Young's modulus of the bearing liner (Polyethylene high density at 20°C [28])	E	Pa	0.9×10^{9}
Poisson's ratio of the bearing liner [28]	σ	—	0.35

Substituting Eq. [13] and [14] into Eq. [7] and collecting the zero and the first-order terms for $\Delta\varepsilon$ and $\varepsilon_0\,\Delta\phi$, a set of coupled partial differential equations in $\tilde{p}_0$, $\tilde{Q}_\varepsilon$, and $\tilde{Q}_\phi$ can be obtained:

$$\Re(\tilde{p}_0) = \frac{1}{2}\frac{\partial \tilde{h}_0}{\partial\theta}, \qquad [17]$$

$$\Re(\tilde{Q}_\varepsilon) = -\frac{3}{2}\frac{(\cos\theta+\tilde{U}_\varepsilon)}{\tilde{h}_0}\frac{\partial\tilde{h}_0}{\partial\theta}+\frac{1}{2}\left(-\sin\theta+\frac{\partial\tilde{U}_\varepsilon}{\partial\theta}\right)+i\gamma\left(\cos\theta+\tilde{U}_\varepsilon\right) - 3\tilde{h}_0\left[\frac{\left(\tilde{h}_0\left(-\sin\theta+\frac{\partial\tilde{U}_\varepsilon}{\partial\theta}\right)-\frac{\partial\tilde{h}_0}{\partial\theta}(\cos\theta+\tilde{U}_\varepsilon)\right)}{12}\frac{\partial\tilde{p}_0}{\partial\theta} + (\mathrm{R/L})^2\frac{\left(\tilde{h}_0\frac{\partial\tilde{U}_\varepsilon}{\partial\tilde{z}}-(\cos\theta+\tilde{U}_\varepsilon)\frac{\partial\tilde{h}_0}{\partial\tilde{z}}\right)}{12}\frac{\partial\tilde{p}_0}{\partial\tilde{z}}\right], \qquad [18]$$

$$\Re(\tilde{Q}_\phi) = -\frac{3}{2}\frac{(\sin\theta+\tilde{U}_\phi)}{\tilde{h}_0}\frac{\partial\tilde{h}_0}{\partial\theta}+\frac{1}{2}\left(\cos\theta+\frac{\partial\tilde{U}_\phi}{\partial\theta}\right)+i\gamma(\sin\theta+\tilde{U}_\phi) - 3\tilde{h}_0\left[\frac{\left(\tilde{h}_0\left(\cos\theta+\frac{\partial\tilde{U}_\phi}{\partial\theta}\right)-\frac{\partial\tilde{h}_0}{\partial\theta}(\sin\theta+\tilde{U}_\phi)\right)}{12}\frac{\partial\tilde{p}_0}{\partial\theta} + (\mathrm{R/L})^2\frac{\left(\tilde{h}_0\frac{\partial\tilde{U}_\phi}{\partial\tilde{z}}-(\sin\theta+\tilde{U}_\phi)\frac{\partial\tilde{h}_0}{\partial\tilde{z}}\right)}{12}\frac{\partial\tilde{p}_0}{\partial\tilde{z}}\right], \qquad [19]$$

where

$$\Re(\bullet) = \frac{\partial}{\partial\theta}\left(\frac{\tilde{h}_0^3}{12}\frac{\partial(\bullet)}{\partial\theta}\right)+(R/L)^2\frac{\partial}{\partial\tilde{z}}\left(\frac{\tilde{h}_0^3}{12}\frac{\partial(\bullet)}{\partial\tilde{z}}\right).$$

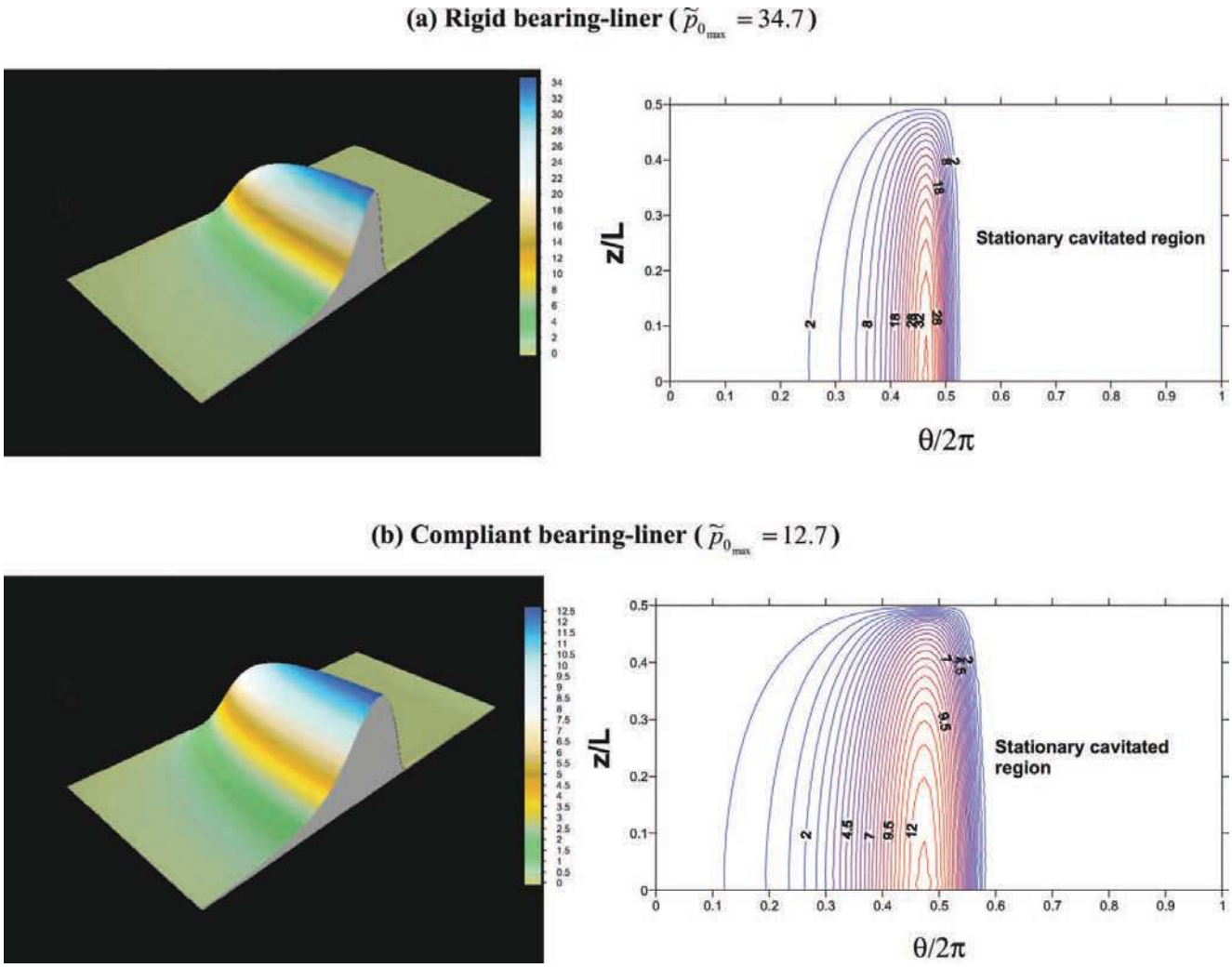

Fig. 6—Steady-state pressure distributions for rigid and compliant journal bearings, $\varepsilon_0 = 0.9$.

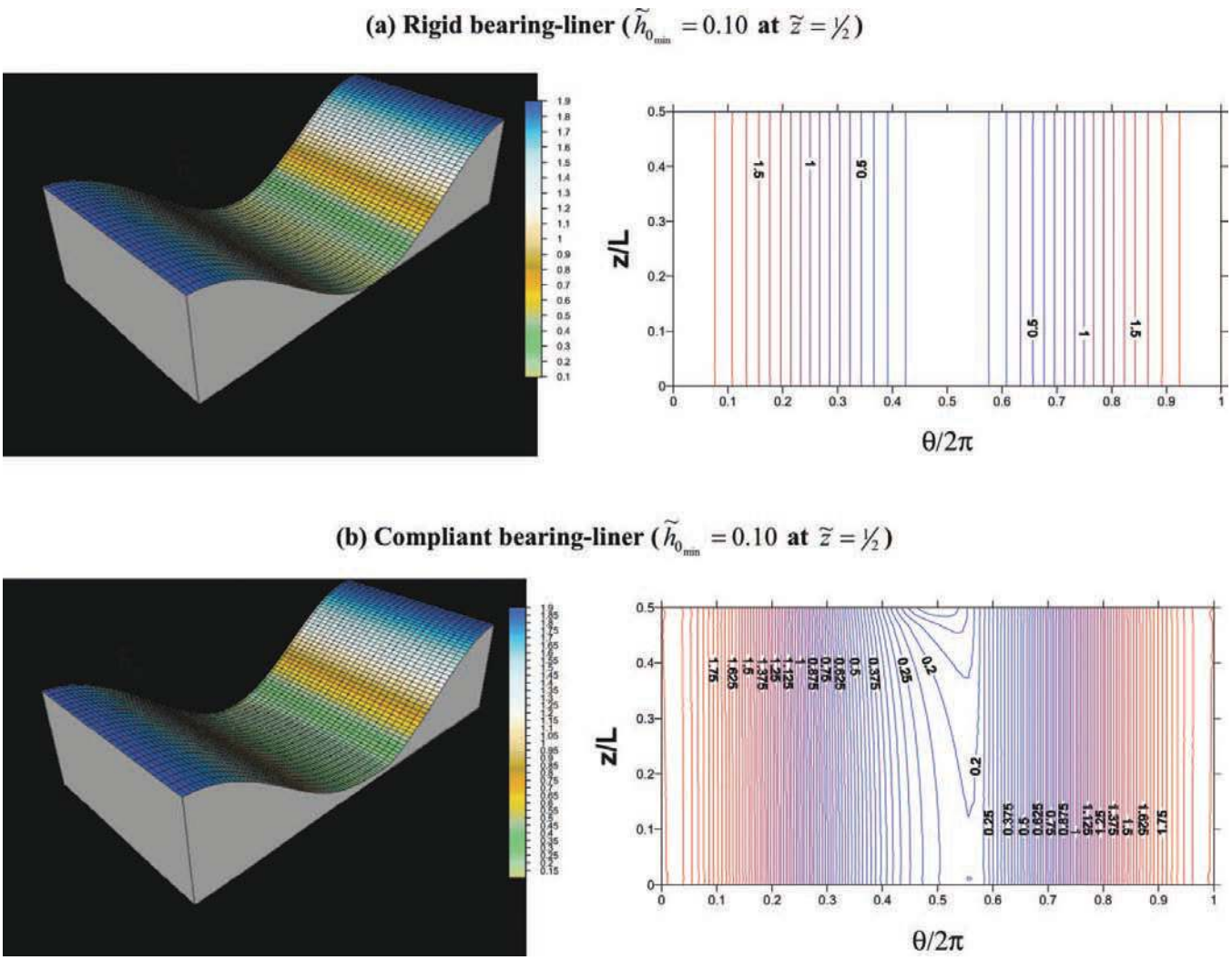

Fig. 7—Steady-state film thickness distributions for rigid and compliant journal bearings, $\varepsilon_0 = 0.9$.

Note that the application of the first-order perturbation technique, which is considered as a superposition method, leads to a transformation of the transient Reynolds equation (Eq. [7]) into three partial differential equations. It is also noteworthy that Eq. [17] is a nonlinear equation because $\tilde{h}_0$ depends on $\tilde{p}_0$, while complex Eq. [18] and [19] are linear in $\tilde{Q}_\varepsilon$ and $\tilde{Q}_\phi$.

The perturbation technique also transforms the boundary conditions of Eq. [8], [9], and [10], i.e.,

$$\tilde{p}_0 = 0 \text{ at } \tilde{z} = \pm 1/2, \quad [20]$$

$$\tilde{p}_0(\theta = 0, \tilde{z}) = \tilde{p}_0(\theta = 2\pi, \tilde{z}), \quad [21]$$

$$\tilde{p}_0 = \frac{\partial \tilde{p}_0}{\partial \theta} = \frac{\partial \tilde{p}_0}{\partial \tilde{z}} = 0 \text{ at } \theta = \theta_{c_0}(\tilde{z}), \quad [22]$$

where θ_{c_0} is the stationary cavitation angle measured from the line of centers.

$$\tilde{Q}_\varepsilon = \tilde{Q}_\phi = 0 \text{ at } \tilde{z} = \pm 1/2, \quad [23]$$

$$\tilde{Q}_\varepsilon(\theta = 0, \tilde{z}) = \tilde{Q}_\phi(\theta = 2\pi, \tilde{z}). \quad [24]$$

Equation [22] expresses the steady-state Reynolds boundary conditions by assuming that the perturbations due to the journal vibrations do not affect the active zone extent. The first-order dynamic equations are therefore solved in the film domain iteratively defined by applying the Christopherson's method in the stationary case.

It is interesting to note that Eq. [22] is derived from Eq. [10] by expanding the normalized pressure $\tilde{p}(\theta, \tilde{z})$ in a first-order Taylor series in the vicinity of $(\theta_{c_0}, \tilde{z}_0)$, i.e.,

$$\tilde{p}(\theta, \tilde{z}) = \tilde{p}(\theta_{c_0} + \Delta\theta, \tilde{z}_0 + \Delta\tilde{z}) \approx \tilde{p}(\theta_{c_0}, \tilde{z}_0) + \left(\frac{\partial \tilde{p}}{\partial \theta}\right)_0 \Delta\theta + \left(\frac{\partial \tilde{p}}{\partial \tilde{z}}\right)_0 \Delta\tilde{z} = 0. \quad [25]$$

Equation [14] can be written as

$$\tilde{p} = \tilde{p}_0 + \tilde{p}_1, \quad [26]$$

where $|\tilde{p}_1| = |\tilde{Q}e^{i\gamma\tilde{t}}| << \tilde{p}_0$.

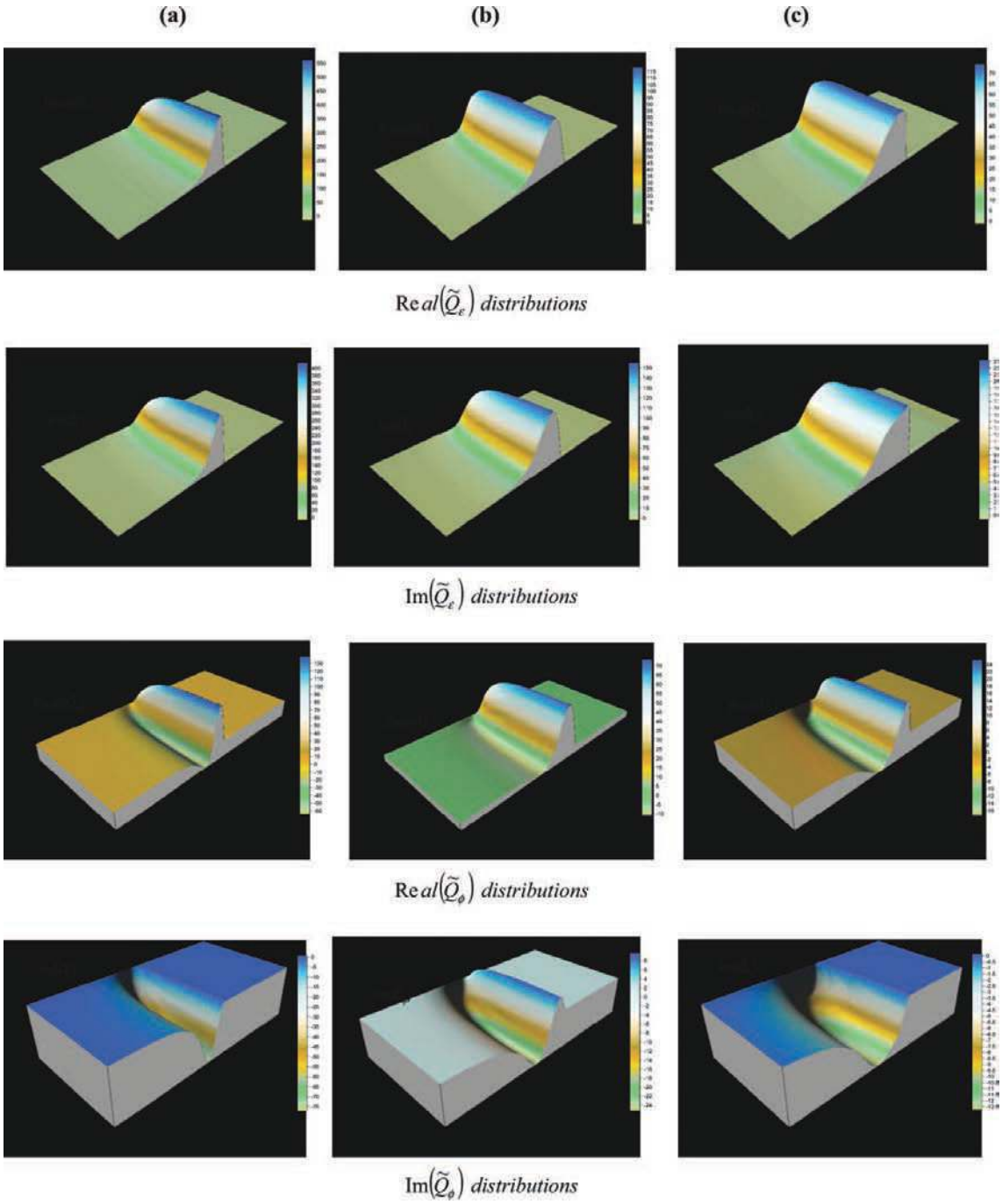

Fig. 8—3-D representations of real and imaginary parts of complex dynamic pressures calculated for rigid and compliant journal bearings, $\varepsilon_0 = 0.9$: (a) Rigid bearing liner, (b) Static deformation, (c) Static and dynamic deformations ($\gamma = 1$).

Substituting Eq. [26] into Eq. [25], we obtain

$$\tilde{p}(\theta, \tilde{z}) \approx \tilde{p}_0(\theta_{c_0}, \tilde{z}_0) + \tilde{p}_1(\theta_{c_0}, \tilde{z}_0) + \left(\frac{\partial \tilde{p}_0}{\partial \theta}\right)_0 \Delta\theta + \left(\frac{\partial \tilde{p}_0}{\partial \tilde{z}}\right)_0 \Delta\tilde{z} = 0. \quad [27]$$

This relation shows that the Reynolds boundary conditions read as

$$\tilde{p}_0 = \frac{\partial \tilde{p}_0}{\partial \theta} = \frac{\partial \tilde{p}_0}{\partial \tilde{z}} = 0, \quad [28]$$

$$\tilde{p}_1 = 0, \text{ i.e., } \tilde{Q}_\varepsilon = \tilde{Q}_\phi = 0. \quad [29]$$

The complex distributions $\tilde{Q}_\varepsilon$ and $\tilde{Q}_\phi$ are obtained from Eq. [18] and [19], from which the eight dynamic coefficients in the

ε, ϕ coordinate system can be calculated by integrations:

$$A_{\varepsilon\varepsilon} + i\gamma B_{\varepsilon\varepsilon} = -\int_0^{2\pi}\int_{-1/2}^{1/2} \tilde{Q}_\varepsilon \cos\theta \, d\tilde{z} d\theta; \; A_{\varepsilon\phi} + i\gamma B_{\varepsilon\phi}$$
$$= -\int_0^{2\pi}\int_{-1/2}^{1/2} \tilde{Q}_\phi \cos\theta \, d\tilde{z} d\theta, \qquad [29a]$$
$$A_{\phi\varepsilon} + i\gamma B_{\phi\varepsilon} = -\int_0^{2\pi}\int_{-1/2}^{1/2} \tilde{Q}_\varepsilon \sin\theta \, d\tilde{z} d\theta; \; A_{\phi\phi} + i\gamma B_{\phi\phi}$$
$$= -\int_0^{2\pi}\int_{-1/2}^{1/2} \tilde{Q}_\phi \sin\theta \, d\tilde{z} d\theta,$$

where

$$A_{\alpha\beta} = a_{\alpha\beta}\frac{C^3}{\mu\omega R^3 L} \text{ and } B_{\alpha\beta} = b_{\alpha\beta}\frac{C^3}{\mu R^3 L}; \; (\alpha, \beta) = (\varepsilon, \phi).$$

The first subscript of $A_{\alpha\beta}$ denotes the direction of the hydrodynamic force, and the second one denotes the direction of displacement. For $B_{\alpha\beta}$, the first and second subscripts refer to the component of the hydrodynamic force and the direction of the velocity, respectively.

The dimensionless stiffness and damping coefficients in the X, Y coordinate system can be calculated from the stiffness and damping coefficients in the ε, ϕ coordinate system according to

$$\begin{bmatrix} A_{XX} & A_{XY} \\ A_{YX} & A_{YY} \end{bmatrix} = \mathbf{R}^T \begin{bmatrix} A_{\varepsilon\varepsilon} & A_{\varepsilon\phi} \\ A_{\phi\varepsilon} & A_{\phi\phi} \end{bmatrix} \mathbf{R}, \qquad [30a]$$

$$\begin{bmatrix} B_{XX} & B_{XY} \\ B_{YX} & B_{YY} \end{bmatrix} = \mathbf{R}^T \begin{bmatrix} B_{\varepsilon\varepsilon} & B_{\varepsilon\phi} \\ B_{\phi\varepsilon} & B_{\phi\phi} \end{bmatrix} \mathbf{R}, \qquad [30b]$$

where the rotation matrix is defined by

$$\mathbf{R} = \begin{bmatrix} \cos\phi_0 & \sin\phi_0 \\ -\sin\phi_0 & \cos\phi_0 \end{bmatrix}.$$

The dimensionless stability parameters (critical mass $\tilde{M}_c$ and whirl frequency ratio γ_c) of the journal-bearing system can be determined at the threshold of instability by applying the Lund's stability criterion *(25)*. The procedure of calculation of the stability parameters is outlined in the next section.

NUMERICAL ANALYSIS

In the present investigation, the partial differential equations (Eq. [17], Eq. [18], Eq. [19]) are solved satisfying the corresponding boundary conditions by finite difference method with successive over-relaxation scheme. Because of the axial symmetry of the bearing, only the half bearing is divided into $N_\theta \times N_z$ equal rectangular cells with an area equal to $\Delta\theta \times \Delta\tilde{z}$, where

$$\Delta\theta = \frac{2\pi}{N_\theta} \text{ and } \Delta\tilde{z} = \frac{0.5}{N_z}.$$

are the mesh sizes in the circumferential and axial directions, respectively (Fig. 4).

Using the accurate central difference approximation for the pressures' partial derivatives, Eq. [17], Eq. [18], and Eq. [19] become the following:

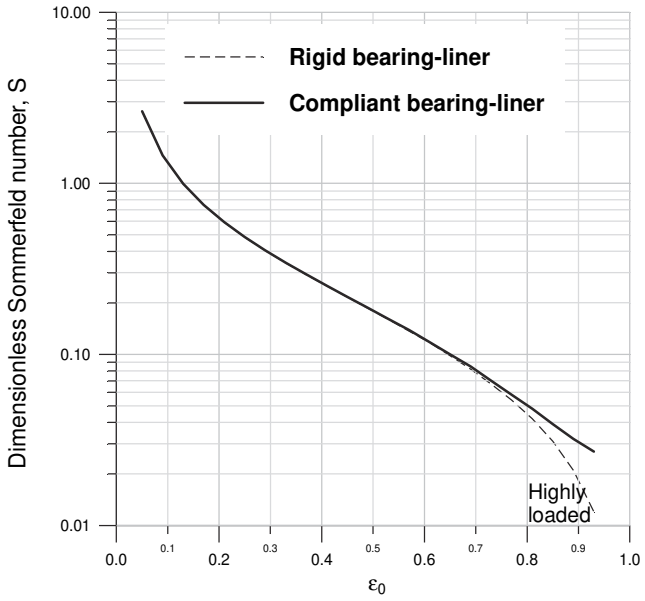

Fig. 9—Variation of Sommerfeld number as a function of steady-state eccentricity ratio.

1. Static governing equation:

$$\tilde{p}_{0_{ij}} = a_{ij}^{(0)}\tilde{p}_{0_{i+1,j}} + b_{ij}^{(0)}\tilde{p}_{0_{i-1,j}} + c_{ij}^{(0)}\tilde{p}_{0_{i,j+1}} + d_{ij}^{(0)}\tilde{p}_{0_{i,j-1}} - e_{ij}^{(0)}, \qquad [31]$$

where

$$a_{ij}^{(0)} = \frac{\frac{h_{0_{ij}}^3}{(\Delta\theta)^2} + \frac{3\bar{h}_{0_{ij}}^2\left(\frac{\partial\bar{h}_0}{\partial\theta}\right)_{ij}}{2\Delta\theta}}{\frac{2h_{0_{ij}}^3}{(\Delta\theta)^2} + 2(R/L)^2\frac{h_{0_{ij}}^3}{(\Delta\tilde{z})^2}}; \; b_{ij}^{(0)} = \frac{\frac{h_{0_{ij}}^3}{(\Delta\theta)^2} - \frac{3\bar{h}_{0_{ij}}^2\left(\frac{\partial\bar{h}_0}{\partial\theta}\right)_{ij}}{2\Delta\theta}}{\frac{2h_{0_{ij}}^3}{(\Delta\theta)^2} + 2(R/L)^2\frac{h_{0_{ij}}^3}{(\Delta\tilde{z})^2}};$$

$$c_{ij}^{(0)} = \frac{(R/L)^2\left(\frac{h_{0_{ij}}^3}{(\Delta\tilde{z})^2} + \frac{3\bar{h}_{0_{ij}}^2\left(\frac{\partial\bar{h}_0}{\partial\tilde{z}}\right)_{ij}}{2\Delta\tilde{z}}\right)}{\frac{2h_{0_{ij}}^3}{(\Delta\theta)^2} + 2(R/L)^2\frac{h_{0_{ij}}^3}{(\Delta\tilde{z})^2}};$$

$$d_{ij}^{(0)} = \frac{(R/L)^2\left(\frac{h_{0_{ij}}^3}{(\Delta\tilde{z})^2} - \frac{3\bar{h}_{0_{ij}}^2\left(\frac{\partial\bar{h}_0}{\partial\tilde{z}}\right)_{ij}}{2\Delta\tilde{z}}\right)}{\frac{2h_{0_{ij}}^3}{(\Delta\theta)^2} + 2(R/L)^2\frac{h_{0_{ij}}^3}{(\Delta\tilde{z})^2}};$$

$$e_{ij}^{(0)} = \frac{6\left(\frac{\partial\bar{h}_0}{\partial\theta}\right)_{ij}}{\frac{2h_{0_{ij}}^3}{(\Delta\theta)^2} + 2(R/L)^2\frac{h_{0_{ij}}^3}{(\Delta\tilde{z})^2}}; \text{ and } \left(\frac{\partial\tilde{h}_0}{\partial\theta}\right)_{ij} \approx \frac{\tilde{h}_{0_{i+1,j}} - \tilde{h}_{0_{i-1,j}}}{2\Delta\theta};$$

$$\left(\frac{\partial\tilde{h}_0}{\partial\tilde{z}}\right)_{ij} \approx \frac{\tilde{h}_{0_{i,j+1}} - \tilde{h}_{0_{i,j-1}}}{2\Delta\tilde{z}};$$

2. Dynamic governing equations:

$$\tilde{Q}_{\varepsilon_{ij}} = a_{ij}^{(\varepsilon)}\tilde{Q}_{\varepsilon_{i+1,j}} + b_{ij}^{(\varepsilon)}\tilde{Q}_{\varepsilon_{i-1,j}} + c_{ij}^{(\varepsilon)}\tilde{Q}_{\varepsilon_{i,j+1}} + d_{ij}^{(\varepsilon)}\tilde{Q}_{\varepsilon i}, j-1 - e_{ij}^{(\varepsilon)}, \qquad [32]$$

$$\tilde{Q}_{\phi_{ij}} = a_{ij}^{(\phi)}\tilde{Q}_{\phi_{i+1,j}} + b_{ij}^{(\phi)}\tilde{Q}_{\phi_{i-1,j}} + c_{ij}^{(\phi)}\tilde{Q}_{\phi_{i,j+1}} + d_{ij}^{(\phi)}\tilde{Q}_{\phi_{i,j-1}} - e_{ij}^{(\phi)}, \quad [33]$$

where

$$a_{ij}^{(\varepsilon)} = \frac{\frac{h_{0_{ij}}^3}{(\Delta\theta)^2} + \frac{3\tilde{h}_{0_{ij}}^2\left(\frac{\partial\tilde{h}_0}{\partial\theta}\right)_{ij}}{2\Delta\theta} + \frac{\tilde{L}_0}{2\Delta\theta}\left(3\tilde{h}_{0_{ij}}^2\left(\frac{\partial\tilde{p}_0}{\partial\theta}\right)_{ij} - 6\right)}{\frac{2h_{0_{ij}}^3}{(\Delta\theta)^2} + 2(R/L)^2\frac{h_{0_{ij}}^3}{(\Delta\tilde{z})^2} + \tilde{L}_0\left(-18\frac{\left(\frac{\partial\tilde{h}_0}{\partial\theta}\right)_{ij}}{\tilde{h}_{0_{ij}}} + 12i\gamma + 3\tilde{h}_{0_{ij}}\left(\frac{\partial\tilde{h}_0}{\partial\theta}\right)_{ij}\left(\frac{\partial\tilde{p}_0}{\partial\theta}\right)_{ij} + 3(R/L)^2\tilde{h}_{0_{ij}}\left(\frac{\partial\tilde{h}_0}{\partial\tilde{z}}\right)_{ij}\left(\frac{\partial\tilde{p}_0}{\partial\tilde{z}}\right)_{ij}\right)}$$

$$b_{ij}^{(\varepsilon)} = \frac{\frac{h_{0_{ij}}^3}{(\Delta\theta)^2} - \frac{3\tilde{h}_{0_{ij}}^2\left(\frac{\partial\tilde{h}_0}{\partial\theta}\right)_{ij}}{2\Delta\theta} + \frac{\tilde{L}_0}{2\Delta\theta}\left(-3\tilde{h}_{0_{ij}}^2\left(\frac{\partial\tilde{p}_0}{\partial\theta}\right)_{ij} + 6\right)}{\frac{2h_{0_{ij}}^3}{(\Delta\theta)^2} + 2(R/L)^2\frac{h_{0_{ij}}^3}{(\Delta\tilde{z})^2} + \tilde{L}_0\left(-18\frac{\left(\frac{\partial\tilde{h}_0}{\partial\theta}\right)_{ij}}{\tilde{h}_{0_{ij}}} + 12i\gamma + 3\tilde{h}_{0_{ij}}\left(\frac{\partial\tilde{h}_0}{\partial\theta}\right)_{ij}\left(\frac{\partial\tilde{p}_0}{\partial\theta}\right)_{ij} + 3(R/L)^2\tilde{h}_{0_{ij}}\left(\frac{\partial\tilde{h}_0}{\partial\tilde{z}}\right)_{ij}\left(\frac{\partial\tilde{p}_0}{\partial\tilde{z}}\right)_{ij}\right)}$$

$$c_{ij}^{(\varepsilon)} = \frac{(R/L)^2\left(\frac{h_{0_{ij}}^3}{(\Delta\tilde{z})^2} + \frac{3\tilde{h}_{0_{ij}}^2\left(\frac{\partial\tilde{h}_0}{\partial\tilde{z}}\right)_{ij}}{2\Delta\tilde{z}} + \frac{3\tilde{L}_0\tilde{h}_{0_{ij}}^2\left(\frac{\partial\tilde{p}_0}{\partial\tilde{z}}\right)_{ij}}{2\Delta\tilde{z}}\right)}{\frac{2h_{0_{ij}}^3}{(\Delta\theta)^2} + 2(R/L)^2\frac{h_{0_{ij}}^3}{(\Delta\tilde{z})^2} + \tilde{L}_0\left(-18\frac{\left(\frac{\partial\tilde{h}_0}{\partial\theta}\right)_{ij}}{\tilde{h}_{0_{ij}}} + 12i\gamma + 3\tilde{h}_{0_{ij}}\left(\frac{\partial\tilde{h}_0}{\partial\theta}\right)_{ij}\left(\frac{\partial\tilde{p}_0}{\partial\theta}\right)_{ij} + 3(R/L)^2\tilde{h}_{0_{ij}}\left(\frac{\partial\tilde{h}_0}{\partial\tilde{z}}\right)_{ij}\left(\frac{\partial\tilde{p}_0}{\partial\tilde{z}}\right)_{ij}\right)}$$

$$d_{ij}^{(\varepsilon)} = \frac{(R/L)^2\left(\frac{h_{0_{ij}}^3}{(\Delta\tilde{z})^2} - \frac{3\tilde{h}_{0_{ij}}^2\left(\frac{\partial\tilde{h}_0}{\partial\tilde{z}}\right)_{ij}}{2\Delta\tilde{z}} - \frac{3\tilde{L}_0\tilde{h}_{0_{ij}}^2\left(\frac{\partial\tilde{p}_0}{\partial\tilde{z}}\right)_{ij}}{2\Delta\tilde{z}}\right)}{\frac{2h_{0_{ij}}^3}{(\Delta\theta)^2} + 2(R/L)^2\frac{h_{0_{ij}}^3}{(\Delta\tilde{z})^2} + \tilde{L}_0\left(-18\frac{\left(\frac{\partial\tilde{h}_0}{\partial\theta}\right)_{ij}}{\tilde{h}_{0_{ij}}} + 12i\gamma + 3\tilde{h}_{0_{ij}}\left(\frac{\partial\tilde{h}_0}{\partial\theta}\right)_{ij}\left(\frac{\partial\tilde{p}_0}{\partial\theta}\right)_{ij} + 3(R/L)^2\tilde{h}_{0_{ij}}\left(\frac{\partial\tilde{h}_0}{\partial\tilde{z}}\right)_{ij}\left(\frac{\partial\tilde{p}_0}{\partial\tilde{z}}\right)_{ij}\right)}$$

$$e_{ij}^{(\varepsilon)} = \frac{-18\cos\theta_i\frac{\left(\frac{\partial\tilde{h}_0}{\partial\theta}\right)_{ij}}{\tilde{h}_{0_{ij}}} - 6\sin\theta_i + 12i\gamma\cos\theta_i + 3\tilde{h}_{0_{ij}}^2\sin\theta_i\left(\frac{\partial\tilde{p}_0}{\partial\theta}\right)_{ij} + 3\tilde{h}_{0_{ij}}\left(\frac{\partial\tilde{h}_0}{\partial\theta}\right)_{ij}\left(\frac{\partial\tilde{p}_0}{\partial\theta}\right)_{ij}\cos\theta_i + 3(R/L)^2\tilde{h}_{0_{ij}}\left(\frac{\partial\tilde{h}_0}{\partial\tilde{z}}\right)_{ij}\left(\frac{\partial\tilde{p}_0}{\partial\tilde{z}}\right)_{ij}\cos\theta_i}{\frac{2h_{0_{ij}}^3}{(\Delta\theta)^2} + 2(R/L)^2\frac{h_{0_{ij}}^3}{(\Delta\tilde{z})^2} + \tilde{L}_0\left(-18\frac{\left(\frac{\partial\tilde{h}_0}{\partial\theta}\right)_{ij}}{\tilde{h}_{0_{ij}}} + 12i\gamma + 3\tilde{h}_{0_{ij}}\left(\frac{\partial\tilde{h}_0}{\partial\theta}\right)_{ij}\left(\frac{\partial\tilde{p}_0}{\partial\theta}\right)_{ij} + 3(R/L)^2\tilde{h}_{0_{ij}}\left(\frac{\partial\tilde{h}_0}{\partial\tilde{z}}\right)_{ij}\left(\frac{\partial\tilde{p}_0}{\partial\tilde{z}}\right)_{ij}\right)}$$

$$a_{ij}^{(\phi)} = a_{ij}^{(\varepsilon)}; \quad b_{ij}^{(\phi)} = b_{ij}^{(\varepsilon)}; \quad c_{ij}^{(\phi)} = c_{ij}^{(\varepsilon)}; \quad d_{ij}^{(\phi)} = d_{ij}^{(\varepsilon)};$$

$$e_{ij}^{(\phi)} = \frac{-18\sin\theta_i\frac{\left(\frac{\partial\tilde{h}_0}{\partial\theta}\right)_{ij}}{\tilde{h}_{0_{ij}}} + 6\cos\theta_i + 12i\gamma\sin\theta_i - 3\tilde{h}_{0_{ij}}^2\cos\theta_i\left(\frac{\partial\tilde{p}_0}{\partial\theta}\right)_{ij} + 3\tilde{h}_{0_{ij}}\left(\frac{\partial\tilde{h}_0}{\partial\theta}\right)_{ij}\left(\frac{\partial\tilde{p}_0}{\partial\theta}\right)_{ij}\sin\theta_i + 3(R/L)^2\tilde{h}_{0_{ij}}\left(\frac{\partial\tilde{h}_0}{\partial\tilde{z}}\right)_{ij}\left(\frac{\partial\tilde{p}_0}{\partial\tilde{z}}\right)_{ij}\sin\theta_i}{\frac{2h_{0_{ij}}^3}{(\Delta\theta)^2} + 2(R/L)^2\frac{h_{0_{ij}}^3}{(\Delta\tilde{z})^2} + \tilde{L}_0\left(-18\frac{\left(\frac{\partial\tilde{h}_0}{\partial\theta}\right)_{ij}}{\tilde{h}_{0_{ij}}} + 12i\gamma + 3\tilde{h}_{0_{ij}}\left(\frac{\partial\tilde{h}_0}{\partial\theta}\right)_{ij}\left(\frac{\partial\tilde{p}_0}{\partial\theta}\right)_{ij} + 3(R/L)^2\tilde{h}_{0_{ij}}\left(\frac{\partial\tilde{h}_0}{\partial\tilde{z}}\right)_{ij}\left(\frac{\partial\tilde{p}_0}{\partial\tilde{z}}\right)_{ij}\right)}$$

and

$$\left(\frac{\partial\tilde{p}_0}{\partial\theta}\right)_{ij} \approx \frac{\tilde{p}_{0_{i+1,j}} - \tilde{p}_{0_{i-1,j}}}{2\Delta\theta}; \left(\frac{\partial\tilde{p}_0}{\partial\tilde{z}}\right)_{ij} \approx \frac{\tilde{p}_{0_{i,j+1}} - \tilde{p}_{0_{i,j-1}}}{2\Delta\tilde{z}}; i = \sqrt{-1}.$$

Applying the successive over-relaxation algorithm, Eq. [31], Eq. [32], and Eq. [33] take the following form:

$$\tilde{p}_{0_{ij}}^{(k+1)} = (1-\Omega)\tilde{p}_{0_{ij}}^{(k)} + \Omega\left(a_{ij}^{(0)}\tilde{p}_{0_{i+1,j}}^{(k)} + b_{ij}^{(0)}\tilde{p}_{0_{i-1,j}}^{(k+1)} + c_{ij}^{(0)}\tilde{p}_{0_{i,j+1}}^{(k)} + d_{ij}^{(0)}\tilde{p}_{0_{i,j-1}}^{(k+1)} - e_{ij}^{(0)}\right) \quad [34a]$$

$$\tilde{Q}_{\varepsilon_{ij}}^{(k+1)} = (1-\Omega)\tilde{Q}_{\varepsilon_{ij}}^{(k)} + \Omega\left(a_{ij}^{(0)}\tilde{Q}_{\varepsilon_{i+1,j}}^{(k)} + b_{ij}^{(0)}\tilde{Q}_{\varepsilon_{i-1,j}}^{(k+1)} + c_{ij}^{(0)}\tilde{Q}_{\varepsilon_{i,j+1}}^{(k)} + d_{ij}^{(0)}\tilde{Q}_{\varepsilon_{i,j-1}}^{(k+1)} - e_{ij}^{(\varepsilon)}\right) \quad [34b]$$

$$\tilde{Q}_{\phi_{ij}}^{(k+1)} = (1-\Omega)\tilde{Q}_{\phi_{ij}}^{(k)} + \Omega\left(a_{ij}^{(0)}\tilde{Q}_{\phi_{i+1,j}}^{(k)} + b_{ij}^{(0)}\tilde{Q}_{\phi_{i-1,j}}^{(k+1)} + c_{ij}^{(0)}\tilde{Q}_{\phi_{i,j+1}}^{(k)} + d_{ij}^{(0)}\tilde{Q}_{\phi_{i,j-1}}^{(k+1)} - e_{ij}^{(\phi)}\right) \quad [34c]$$

where k andΩ are the number of iterations and the relaxation factor, respectively.

Different mesh sizes were tried, and a mesh size with 91×21 grid was adopted. This size gives more accurate results with a rapid rate of convergence when the value of Ω is equal to 1.80. This optimal value, which is predicted by numerical experimentation, will always lie between 1.0 and 2.0 as shown in Fig. 5.

The solution of elastohydrodynamic problem under static and dynamic conditions is obtained by an iterative numerical procedure. The following steps are performed:

1. Select the input parameters of the problem ε_0, R/L,$\tilde{t}_h$,$\tilde{C}_d$,σ ,N_θ, N_z, γ, relaxation factors, convergence criteria, and maximum number of iterations.
2. Compute the undeformed film thickness $\tilde{h}_{0_{ij}}$ from Eq. [5].
3. Initialize the iteration number n to 0.
4. Initialize the dimensionless static pressure field $\tilde{p}_{0_{ij}}^{(n)} = 0$ and the dimensionless static film thickness profile $\tilde{h}_{ij}^{(n)} = \tilde{h}_{0_{ij}}$.

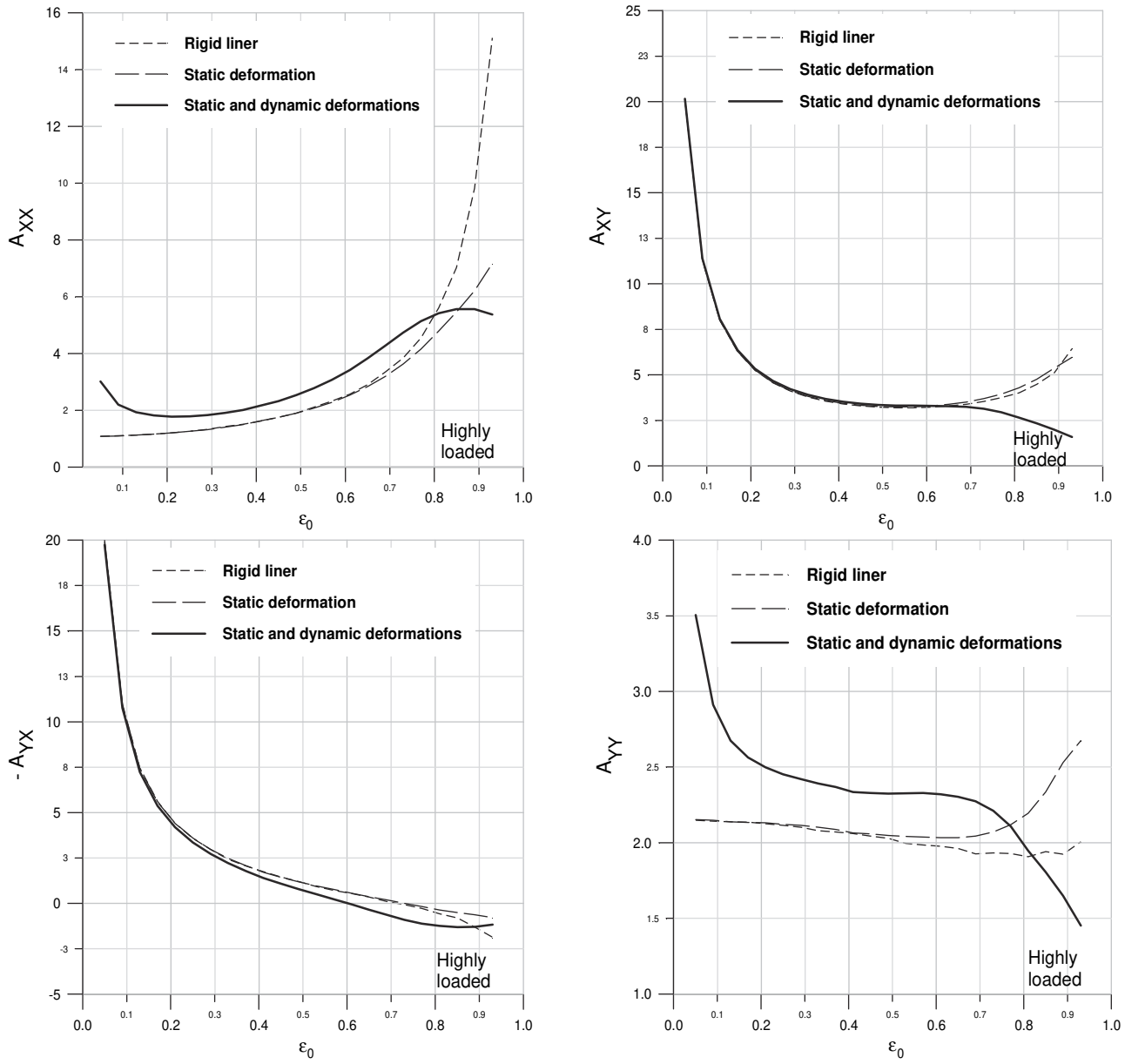

Fig. 10—Fluid-film dimensionless synchronous stiffness coefficients as a function of steady-state eccentricity ratio, $\gamma = 1$.

5. Solve the zeroth-order equation (Eq. [17]) for the static pressure field $\tilde{p}_{0_{ij}}^{(n+1)}$ using the finite difference method with successive over-relaxation scheme. The iterative process is repeated until either the pressure convergence criterion is achieved or the maximum number of iterations is exceeded.
6. Update the dimensionless film thickness profile according to

$$\tilde{h}_{ij}^{(n+1)} = \tilde{h}_{0_{ij}}^{+} \tilde{L}_0 \left((1-\alpha)\tilde{p}_{0_{ij}}^{(n)} + \alpha \tilde{p}_{0_{ij}}^{(n+1)} \right),$$

where α is an under-relaxation factor that ranges from 0 to 1.

7. Check the static film pressure convergence criterion $\frac{1}{N}\sum_{i,j}\left|\frac{\tilde{p}_{0ij}^{(n+1)} - \tilde{p}_{0ij}^{(n)}}{\tilde{p}_{0ij}^{(n+1)}}\right| \leq 10^{-5}$, where N is the total number of nodes for which the pressure is positive. If convergence is not achieved, then increment the iteration number n by 1 and return to step 5.
8. Code the nodes for which the static pressure is positive and calculate the static pressure and film thickness derivatives at each node. This step is necessary to solve the first-order equations Eq. [18] and Eq. [19].
12. Calculate the steady-state hydrodynamic force components and the attitude angle by means of numerical integrations:

$$\begin{Bmatrix} F_{\varepsilon_0} \\ F_{\phi_0} \end{Bmatrix} = 2\int_0^{1/2}\int_0^{\theta_{c_0}} \tilde{p}_0 \begin{Bmatrix} \cos\theta \\ \sin\theta \end{Bmatrix} d\theta d\tilde{z}, \text{ and} \phi_0 = Tan^{-1}\left(-\tilde{F}_{\phi_0}\tilde{F}_{\varepsilon_0}\right). \quad [35]$$

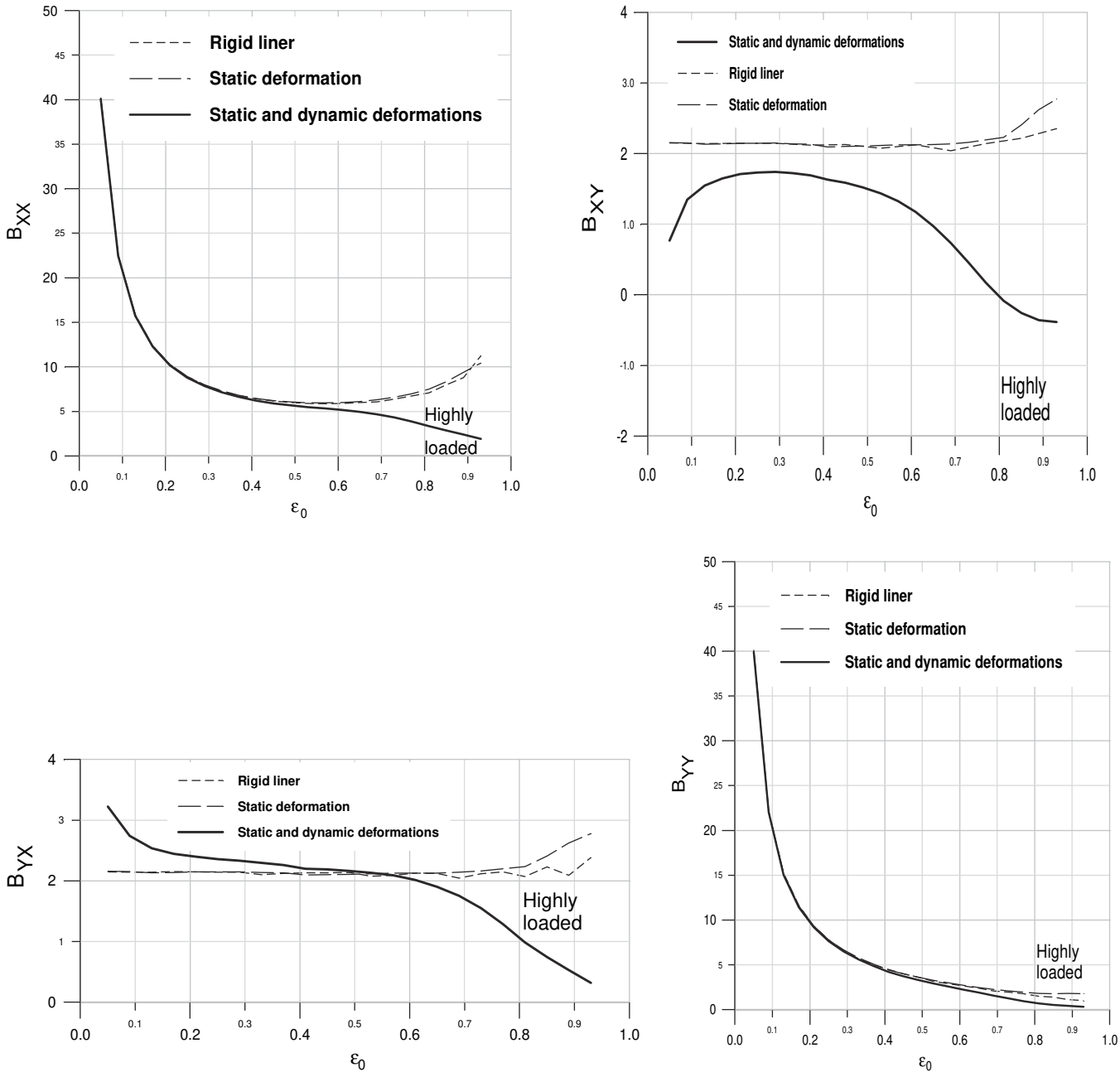

Fig. 11—Fluid-film dimensionless synchronous damping coefficients as a function of steady-state eccentricity ratio, $\gamma = 1$.

13. Solve the first-order equations Eq. [18] and Eq. [19] by the finite difference method with successive over-relaxation scheme to obtain the complex dynamic pressures $\tilde{Q}_{\varepsilon_{ij}}$ and $\tilde{Q}_{\phi_{ij}}$. It should be noted that the calculations are performed for each coded node belonging to the stationary active region without vanishing the computed negative pressure terms. The pressure convergence criterion is similar to that used for the calculation of static pressure.
14. Calculate the eight fluid-film dynamic coefficients (Eq. [29] and Eq. [30]), from which the equivalent stiffness coefficient A_{eq} and whirl frequency ratio γ_c at stability threshold are obtained:

$$A_{eq} = \frac{A_{XX}B_{YY} + A_{YY}B_{XX} - A_{XY}B_{YX} - A_{YX}B_{XY}}{B_{XX} + B_{YY}},$$

$$\gamma_c^2 = \frac{(A_{XX} - A_{eq})(A_{YY} - A_{eq}) - A_{XY}A_{YX}}{B_{XX}B_{YY} - B_{XY}B_{YX}}.$$

Note that there is dependence between dynamic coefficients and frequency ratio when the deformations due to the dynamic pressures at the fluid-film–bearing-liner interface are considered.

15. Test the sign of γ_c^2: If $\gamma_c^2 < 0$, then the equilibrium position is stable *(26)*; otherwise, $\gamma_c^2 > 0$. The dimensionless critical

mass is then calculated:

$$\tilde{M}_c = \frac{A_{eq}}{\gamma_c^2}.$$

16. Test the calculated value of γ_c with γ: If γ_c does not coincide with the estimatedγ, then set $\gamma \leftarrow \gamma_c$, and return to step 13 until convergence is reached with a sufficient accuracy, i.e.,

$$\left|\frac{\gamma - \gamma_c}{\gamma_c}\right| \leq 10^{-4}.$$

RESULTS AND DISCUSSION

Based on the analysis described in the present article, a computer code was developed to study the effects of both static and dynamic deformations on the dynamic behavior of a compliant journal bearing using the linearized theory.

Validation

To validate the static and dynamic results obtained from the computer program, we compared the Sommerfeld number, attitude angle, stiffness and damping coefficients, and the dimensionless stability parameters (critical mass and whirl frequency ratio) for a rigid finite-length journal bearing ($R/L = 0.5$ and$\tilde{C}_d = 0.$) with those published by Constantinescu, et al. *(27)*. The results were obtained for three values of static eccentricity ratio ($\varepsilon_0 =$ 0.0962, 0.5374, and 0.8349). As can be seen in Table 1, the results are in good agreement even at high values of static eccentricity ratio. Furthermore, all dynamic results presented in *(27)* for $R/L =$ 0.25 and 1 were recovered.

Effects of Elastic Deformations on the Steady-State and Dynamic Fluid-Film Pressures

Table 2 shows the details of bearing geometry and operating conditions of a sample problem investigated in the present study. The dimensionless parameters calculated from numerical values given in Table 2 are as follows: $\tilde{C}_d = 0.04$, $\tilde{t}_h = 0.40$, $R/L = 0.5$, $C/R = 2\times10^{-3}$, which are the deformation coefficient, the relative thickness of the bearing liner, and the aspect and clearance ratios of the journal bearing, respectively.

Figure 6 depicts the steady-state pressure profiles and contours calculated in the half bearing for a highly loaded journal bearing operating at $\varepsilon_0 = 0.9$. It is observed that the effect of the bearing-liner elasticity leads to a spreading of the pressure distribution in the circumferential direction of the journal bearing and to an important reduction of the peak pressure inducing a reduction of the journal-bearing carrying capacity.

Figure 7 shows the fluid film thickness distributions obtained for rigid and compliant bearings. In the rigid case, the film thickness has a sinusoidal shape whose minimum value occurs at $\theta =$ 180 degrees regardless of the cross-section of bearing. The film thickness profile calculated by taking into account the compliance of the bearing liner is different from that obtained in the rigid case and presents maximum and minimum values at the midplane section and the free edges of bearing, respectively. The increasing of the film thickness at the midplane section of the journal bearing explains the pressure drop.

Figure 8 compares the real and imaginary parts of complex dynamic pressures $\tilde{Q}_\varepsilon$ and $\tilde{Q}_\phi$ calculated in the half bearing for

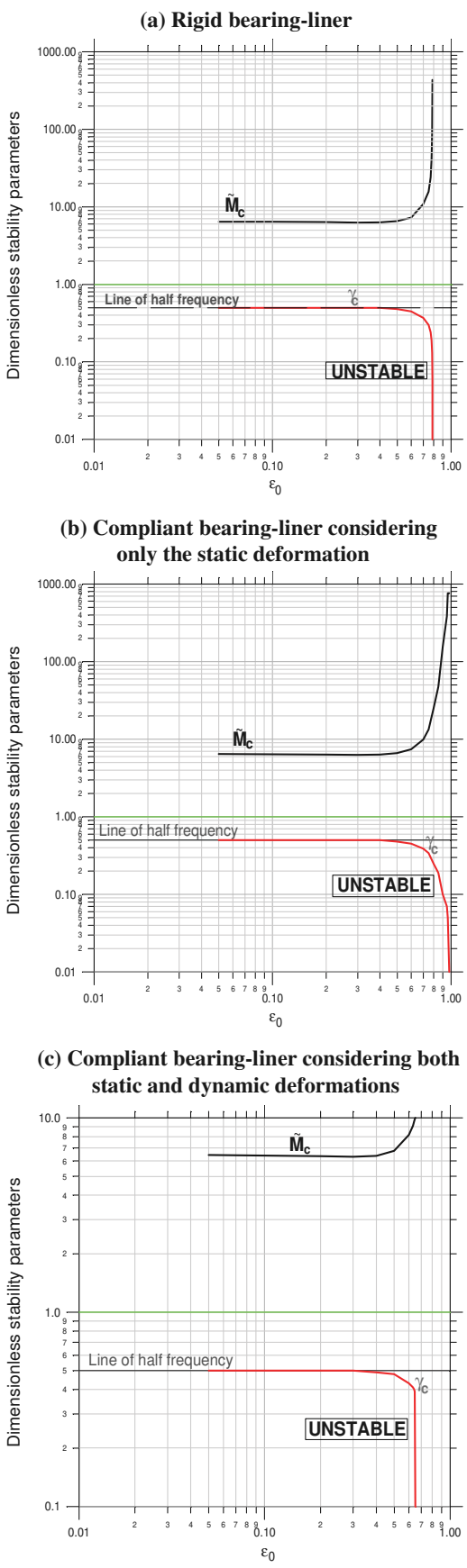

Fig. 12—Stability parameters as functions of steady-state eccentricity ratio.

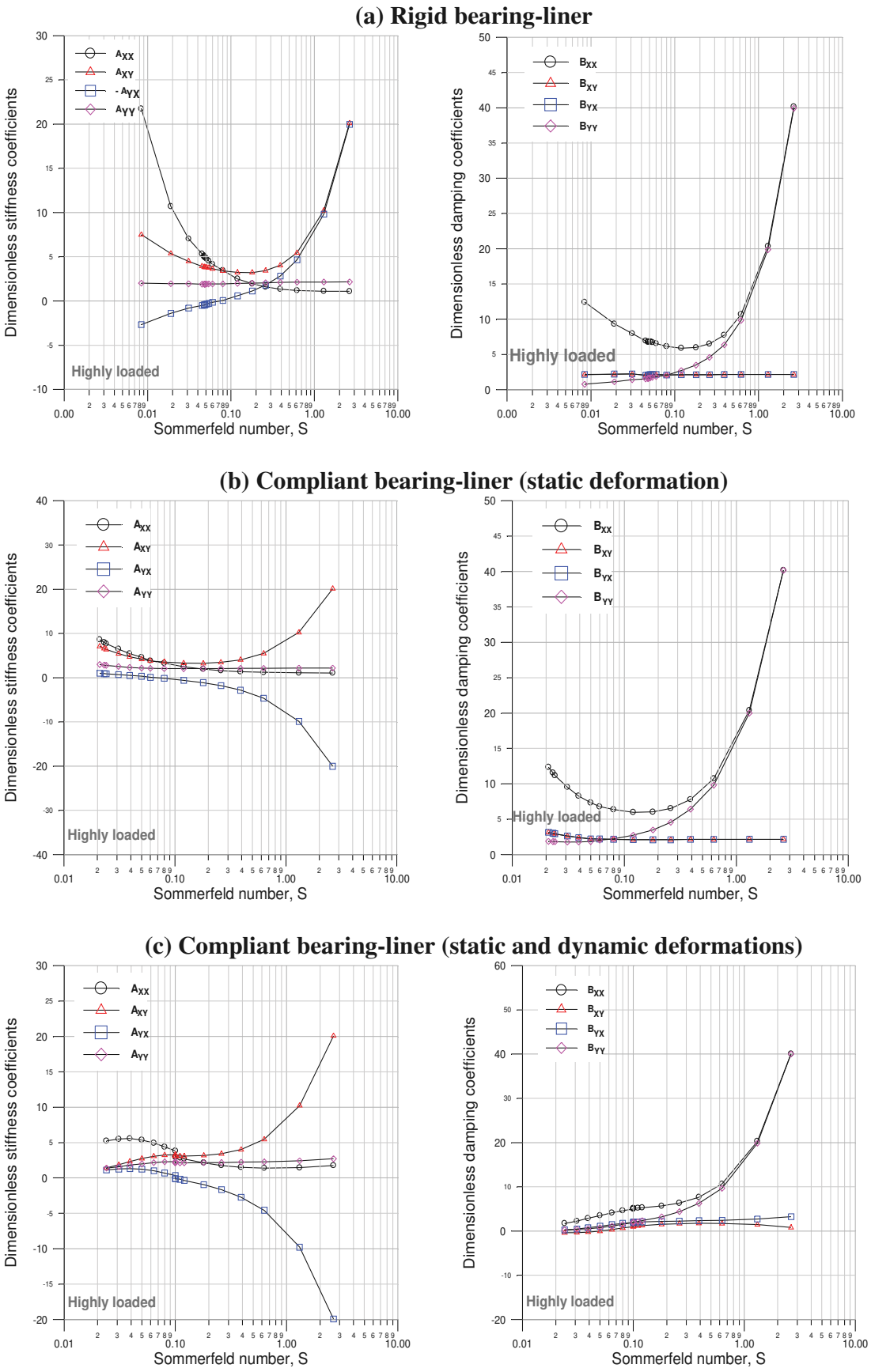

Fig. 13—Stiffness and damping coefficients as functions of Sommerfeld number, $\gamma = \gamma_c$.

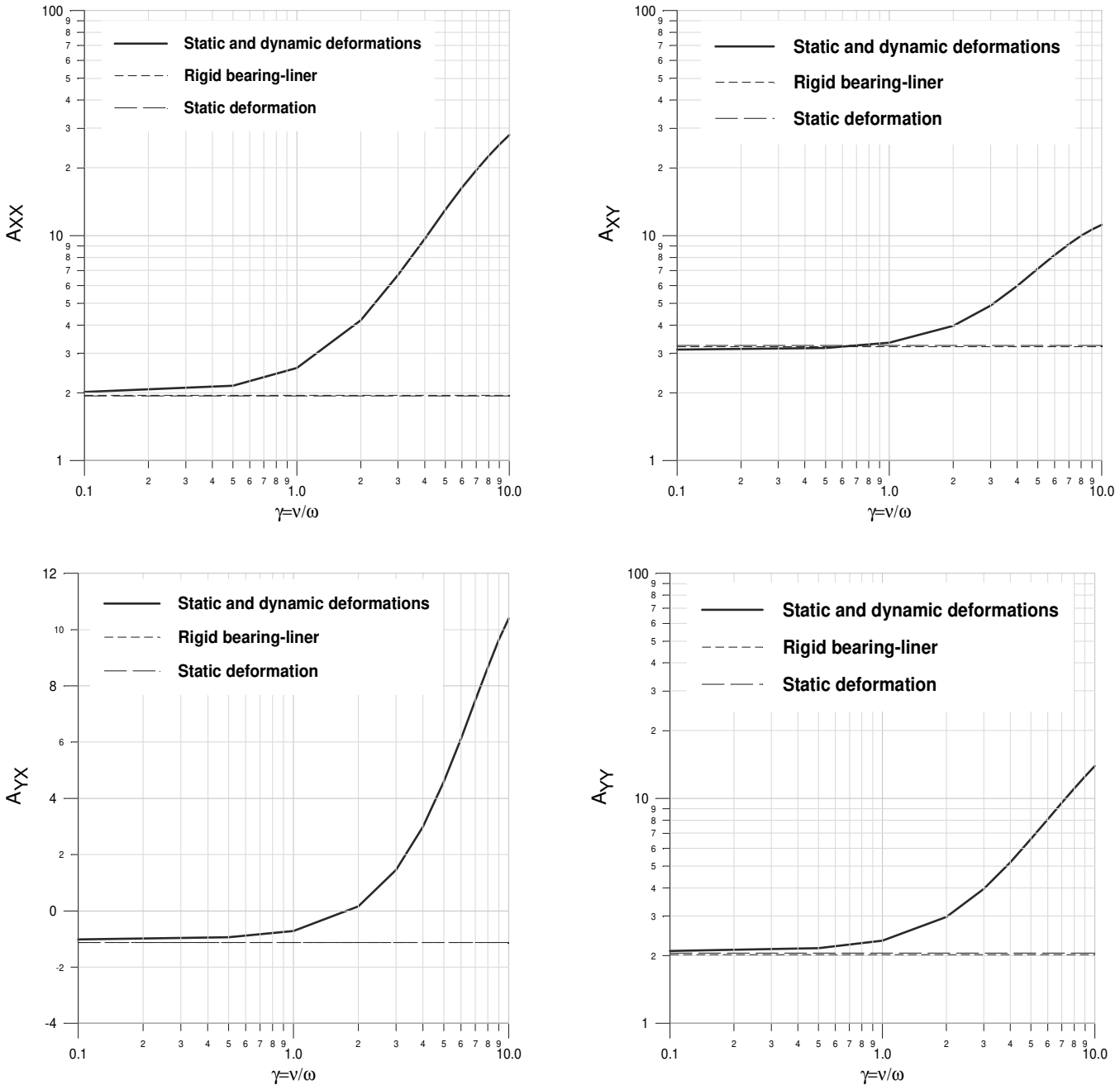

Fig. 14—Dimensionless stiffness coefficients as functions of relative excitation frequency, $\varepsilon_0 = 0, 5$.

rigid and compliant bearing liners and $\varepsilon_0 = 0.9$. As found under steady-state conditions, the elastic deformations also affect the maximum value of both dynamic pressures, and this effect is more pronounced when the dynamic deformations are considered in addition to the static ones.

Influence of Elastic Deformations on the Sommerfeld Number

Evolutions of the dimensionless Sommerfeld number S (also commonly known as the load number) versus the steady-state eccentricity ratio for rigid and elastic bearing liners are depicted in Fig. 9. This number, which represents the inverse of the applied load ($S \to 0$ as$\varepsilon_0 \to 1$), depends on several design parameters, namely the absolute viscosity of lubricant μ, the geometric characteristics of the journal bearing ($R,\ L$ and C) and the operating conditions ω and W_0. It is clearly shown that the elasticity effect on the Sommerfeld number becomes significant when the journal bearing operates at eccentricities greater than 0.80, i.e., when the journal bearing system is moderately or highly loaded.

Influence of Dynamic Deformations on the Dynamic Properties

The graphical results were obtained for three cases:

- rigid bearing-liner case (doted lines),
- compliant bearing liner when only static deformation is considered (dashed lines),

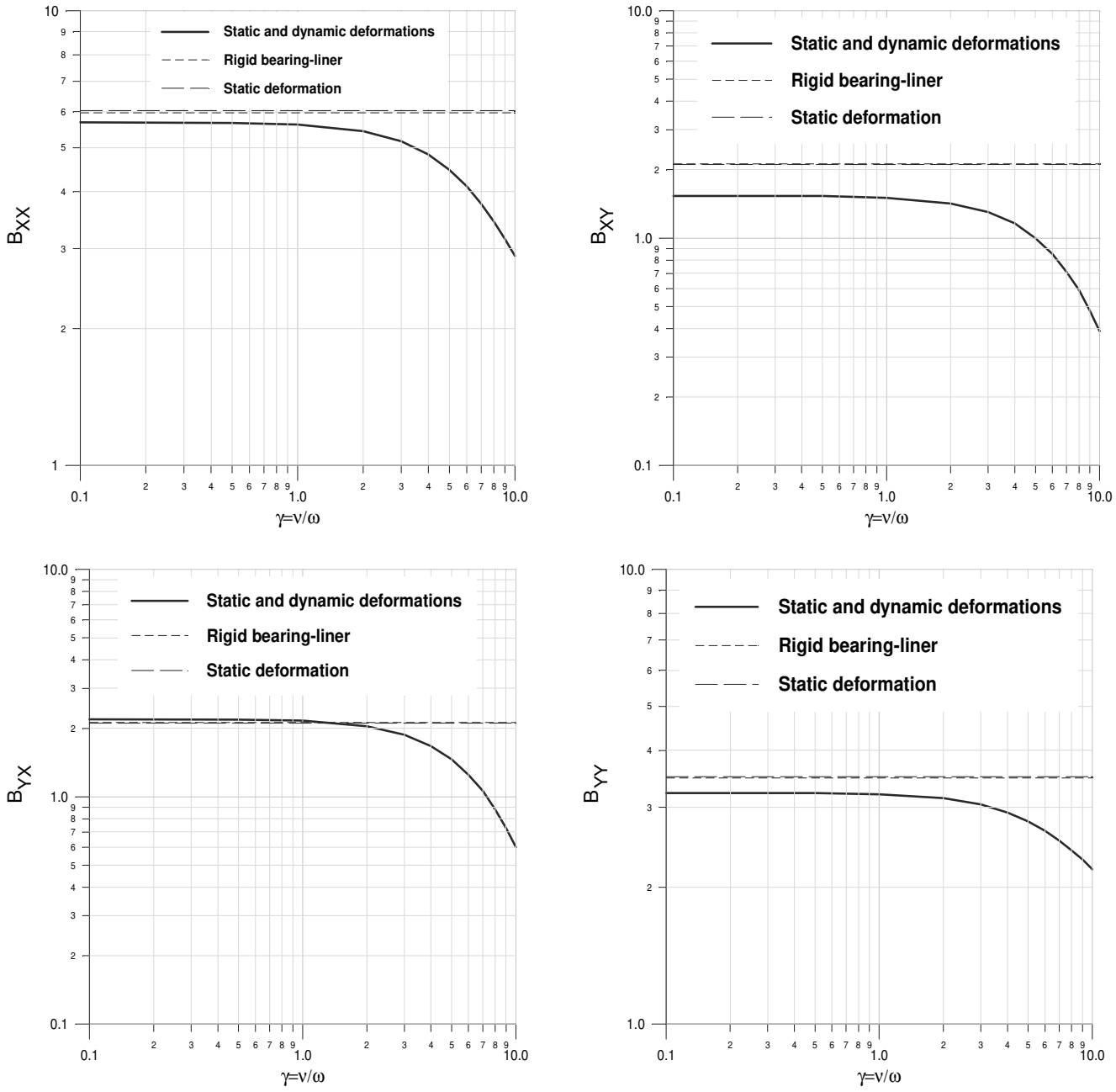

Fig. 15—Dimensionless damping coefficients as a function of relative excitation frequency, $\epsilon_0 = 0, 5$.

- compliant bearing liner when both static and dynamic deformations are considered (solid lines).

Figure 10 shows the variations of the four synchronous dimensionless fluid-film stiffness coefficients with the steady-state eccentricity ratio obtained for both rigid and compliant bearing liners. It is observed that when the dynamic deformation is ignored, the effect of static deformation on stiffness coefficients is significant for eccentricities greater than 0.7.

Consideration of dynamic distortions changes the evolution of the direct stiffness coefficients regardless of the running eccentricity.

The stiffening effect shown in that same figure comes, in our opinion, from the additional pressure (fig. 8) coming from the dynamic deformation. The dynamic movement of the shaft creates additional dynamic pressure leading to an increase of stiffness. At high eccentricity, this phenomenon is counterbalanced by the extent of the positive pressure zone, and thus the maximum pressure magnitude decreases, and the pressure appearance is more flat.

Note that the change of sign from negative to positive for the cross-coupling stiffness coefficient A_{YX} plays a significant role in the stability of system. The figure clearly shows that the A_{YX} change of sign, calculated when both static and dynamic deformations are considered, occurs at an eccentricity ratio around 0.60.

Figure 11 shows the four synchronous dimensionless fluid-film damping coefficients versus the steady-state eccentricity ratio calculated for $\gamma = 1$. It can be observed that the four damping coefficients generally decrease with the journal eccentricity, i.e., when the system is heavily loaded.

Consideration of dynamic distortions changes the evolution of the cross-coupling damping coefficients whatever the running eccentricity is.

Especially, the two cross-coupling damping coefficients' values B_{XY} and B_{YX} differ from each other significantly when dynamic deformation is taken into consideration instead of being equal as predicted by the classical hydrodynamic lubrication theory (see the detailed demonstration in Appendix A) or by the EHD approach when the dynamic deformations are neglected. It should be specified that the dynamic deformation might be one of the main causes of the significant discrepancy between the values of the two cross-coupling damping coefficients determined experimentally by other researchers *(29)*.

Influence of Dynamic Deformations on the Stability Parameters

According to the obtained stiffness and damping coefficients, the critical mass and the whirl ratio of the rigid rotor-bearing system are determined and plotted in Fig. 12. These figures show variations of the aforementioned parameters against the steady-state eccentricity ratio. It is observed that significant reduction of the instability boundary can occur if the effects of both static and dynamic deformations are considered in the calculations because of the enhancement of the fluid-film stiffness coefficients. Figure 13 depicts the variations of fluid-film dynamic coefficients obtained for $\gamma = \gamma_c$ versus Sommerfeld number. Exciting the journal into a harmonic motion of small amplitude at frequency ν gives steady state pressure and complex dynamic pressures Q_ε and Q. Taking into account the dynamic deformation leads to an increase of the real part of $Q_\varepsilon$and Q (see Eq. [18] and Eq. [19]) and the magnitude of the imaginary part. This additional pressure increases the stiffness coefficients by increasing the attitude angle for a given eccentricity. For direct stiffness coefficients, no effects occur until $\varepsilon_0 = 0.6 \approx 0.7$. For crossed coefficients, taking into account the imaginary part plays an immediate role on attitude angle.

Influence of Excitation Frequency on the Stiffness and Dynamic Coefficients

Figures 14 and 15 present respectively dimensionless fluid-film stiffness and damping coefficients as functions of the relative excitation frequency for $\varepsilon_0 = 0.5$. The results show that the dynamic coefficients calculated for rigid and compliant bearing liners considering solely static deformations are independent of the excitation frequency. When both static and dynamic deformations are considered, these coefficients stay mainly constant for low magnitudes of the frequency excitation. However, we observe a nonlinear evolution of these coefficients when considering high-frequency values, which can happen in some machines with gear elements.

CONCLUSIONS

According to the results obtained, the following conclusions can be drawn:

1. The elastic deformations affect the maximum value of both dynamic pressures, and this effect is more pronounced when the dynamic deformations are considered in addition to the static ones.
2. Consideration of dynamic distortions changes the evolution of the direct stiffness coefficients and the cross-coupling damping coefficients, regardless of the running eccentricity.
3. The effects of dynamic deformations of the bearing liner on dynamic performance characteristics and stability parameters are nonnegligible, especially for high values of the operating eccentricity ratio and/or low-elasticity modulus bearing liners.
4. The cross-coupling damping coefficients differ from each other significantly when dynamic deformation is included.
5. It is observed that significant reduction of the instability boundary can occur if the effects of both static and dynamic deformations are considered.
6. At high values of excitation frequency, the fluid-film dynamic coefficients become nonlinear as functions of this frequency.

REFERENCES

(1) Higginson, G. R. (1965–66), "The Theoretical Effects of Elastic Deformation of the Bearing Liner on Journal Bearing Performance." *Proc. of the Symposium on Elastohydrodynamic Lubrication, IMechE*, London (UK), **180**, Part 3B pp 31-38.

(2) O'Donoghue, G., Brighton, D. K. and Hooke, C. J. K. (1967), "The Effect of Elastic Distortions on Journal Bearing Performance." *Journal of Lubrication Technology*, Series F, **89**, 409-417.

(3) Brighton, D. K., Hooke, C. J. K. and O'Donoghue, G. A. (1967–68), "Theoretical and Experimental Investigation of the Effect of Elastic Distortions on the Performance of Journal Bearings." *Proc. IMechE*, 1967–68, **182**, Part 3N, 192-200.

(4) Oh, K. P. and Huebner, K. H. (1973), "Solution of the Elastohydrodynamic Finite Journal Bearing Problem." *Trans. ASME*, July **1973**, 342-352.

(5) Conway, H. D. and Lee, H. C. (1975), "The Analysis of the Lubrication of a Flexible Journal Bearing." *Journal of Lubrication Technology*, **97**, 599-604.

(6) Jain, S. C., Sinhasan, R. and Singh, D. V. (1982), "The Performance Characteristics of Thin Compliant Shell Journal Bearings." *Wear*, **81**, pp 251-261.

(7) Jain, S. C., Sinhasan, R. and Singh, D. V. (1984), "A Study of Elastohydrodynamic Lubrication in a Journal Bearing With Piezoviscous Lubricants." *ASLE Transactions*, **27**, 168-176.

(8) Chandrawat, H. N. and Sinhasan R. A. (1988), "Study of Steady-State and Transient Performance Characteristics of a Flexible Shell Journal Bearing." *Tribology International*, **21**, 137-148.

(9) Majumdar, B. C., Brewe, D. E. and Khonsari, M. M. (1988), "Stability of a Rigid Rotor Supported on Flexible Fluid Journal Bearings." *Journal of Tribology*, **110**, 181-187.

(10) Giudicelli, B., Bou-Saïd, B. and Villechaise, B. (1989), "Running Characteristics of Rubber Coating Bearing," *European Journal of Mechanics A/Solids*, **8**, pp. 361-372.

(11) Braun, M. J. and Dougherty, J. D. (1989), "Hydrodynamic Analysis and Fluid-Solid Interaction Effects on the Behavior of a Compliant Wall (Thick) Journal Bearing. Part 1: Theory." *Transactions of the ASME,* January 1989, **111**, 70-79.

(12) Braun, M. J. and Dougherty, J. D. (1989), "Hydrodynamic Analysis and Fluid-Solid Interaction Effects on the Behavior of a Compliant Wall (Thick) Journal Bearing. Part 2: Results." *Transactions of the ASME,* January 1989, **111**, 80-86.

(13) Mokhiamer, U. M., Crosby, W. A. and El-Gamal, H. A. (1999), "A Study of a Journal Bearing Lubricated by Fluids With Couple-Stress Considering the Elasticity of the Liner." *Wear*, **224**, 194-201.

(14) Lahmar, M., Belbah, A. and Nicolas, D. (2002), "Effets des Déformations Élastiques des Revêtements de Surface sur le Comportement Dynamique

et la Stabilité des Paliers Hydrodynamiques." *Revue Matériaux & Techniques,* SIRPE Editeur: Paris, 11-12, 17-30.
(15) Lahmar, M. (2005), "Elastohydrodynamic Analysis of Double-Layered Journal Bearings Lubricated With Couple-Stress Fluids." *Proc. IMechE, Part J: Journal of Engineering Tribology*, **219**, 145-171.
(16) Boucherit, H., Lahmar, M. and Bou-Saïd, B. (2008), "Misalignment Effects on Steady-State and Dynamic Behavior of Compliant Journal Bearings Lubricated With Couple Stress Fluids," *Lubrication Science,* Wiley Inter-Science, **20**, 241-268.
(17) Lahmar, M., Haddad, A. and Nicolas, D. (2000), "An Optimised Short Bearing Theory for Nonlinear Dynamic Analysis of Turbulent Journal Bearings." *European Journal of Mechanics A/Solids,* **19**, 151-177.
(18) Swift, H. W. (1931), "The Stability of Lubricating Films in Journal Bearings." *J. Inst. Engrs.*, **233**(1), 267-322.
(19) Stieber, W. (1933), "Das Schwimmlajer, Hydrodynamische Theori des Glutlajers," VDI: Berlin.
(20) Christopherson, D. G. (1941), "A New Mathematical Method for the Solution of Oil Film Lubrication Problems." *Proc. IMechE,* **141**, 126-135.
(21) Bayada, G. and Chambat, M. (1986), "Sur Quelques Modélisations de la Zone de Cavitation en Lubrification Hydrodynamique." *Journal de Mécanique Théorique et Appliquée,* **5**(5), 703-729.
(22) Bayada, G. (1972), "Inéquations Variationnelles à Conditions aux Limites Périodiques." Thèse présentée devant l'université de Lyon I.
(23) Dowson, D. and Taylor, C. M. (1979), "Cavitation in Bearings." *Ann. Rev. Fluid Mech.,* **11**, 35-66.
(24) Jain, S. C., Sinhasan, R. and Pilli, S. C. (1989), "A Study on the Dynamic Response of Compliant Shell Journal Bearings," *Tribology Transactions,* **32**(3), 297-304.
(25) Lund, J. W. (1986), "Review of the Concept of Dynamic Coefficients for Fluid Film Journal Bearings," *Journal of Tribology, Trans. of the ASME*, 1986.
(26) Frêne, J., Nicolas, D., Degueurce, B., Berth, D. and Godet, M. (1997), "Hydrodynamic Lubrication: Bearings and Thrust Bearings," Elsevier: Maryland Heights, MO.
(27) Constantinescu, V. N., Nica, Al., Pascovici, M. D., Ceptureanu, G. and Nedelcu, S. (1985), "Sliding Bearings," Allerton Press: New York.
(28) Hamrock, B. J., Schmid, S. R. and Jacobson, B. O. (2004), "Fundamentals of Fluid Film Lubrication," Second Edition, Marcel Dekker: New York, 145-147.
(29) Piteau, P. and Debailleux, C. (1990), "Banc d'Essais de Paliers: Mesure des Coefficients Dynamiques d'un palier circulaire," *Journées de la Société Française de Tribologie (S. F. T.),* La tribologie dans les machines tournantes, Poitiers, France, April 4-5, 1990.

APPENDIX A SYMMETRY OF THE FLUID-FILM DAMPING MATRIX

To demonstrate the property of symmetry of the rigid hydrodynamic journal bearings damping matrix, it is convenient to write the Reynolds equation (Eq. [6]) in the form

$$\frac{1}{R^2}\frac{\partial}{\partial\theta}\left(\frac{h^3}{12\mu}\frac{\partial p}{\partial\theta}\right)+\frac{\partial}{\partial z}\left(\frac{h^3}{12\mu}\frac{\partial p}{\partial z}\right) = \frac{1}{2}\left[(\omega-2\dot{\phi})\frac{\partial h}{\partial\theta}+2\dot{e}\cos\theta\right], \qquad [A1]$$

where

$$h = C(1+\varepsilon\cos\theta), \quad \frac{\partial h}{\partial\theta} = -C\varepsilon\sin\theta, \text{ and } (^{\bullet}) = \frac{d()}{dt},$$

or in its dimensionless form,

$$\Re(\tilde{p}) = \frac{1}{2}\frac{\partial\tilde{h}}{\partial\theta}+\frac{\varepsilon'\cos\theta}{1-2\phi'}, \qquad [A2]$$

where

$$\tilde{h} = \frac{h}{C}, \quad \tilde{p} = \frac{p}{\mu\omega(R/C)^2(1-2\phi')}, \quad \tilde{z} = \frac{z}{L}, \quad \tilde{t} = \omega t,$$

$$()' = \frac{d()}{d\tilde{t}} = \frac{1}{\omega}(^{\bullet}),$$

and

$$\Re(\bullet) = \frac{\partial}{\partial\theta}\left(\frac{\tilde{h}^3}{12}\frac{\partial}{\partial\theta}(\bullet)\right)+(R/L)^2\frac{\partial}{\partial\tilde{z}}\left(\frac{\tilde{h}^3}{12}\frac{\partial}{\partial\tilde{z}}(\bullet)\right).$$

The radial and tangential fluid film forces are expressed as

$$\begin{Bmatrix}F_\varepsilon\\F_\phi\end{Bmatrix} = \int_{-L/2}^{L/2}\int_{\theta_1}^{\theta_2} p\begin{Bmatrix}\cos\theta\\\sin\theta\end{Bmatrix}Rd\theta dz = \eta\omega(1-2\phi')\int_{-1/2}^{1/2}\int_{\theta_1}^{\theta_2}\tilde{p}\begin{Bmatrix}\cos\theta\\\sin\theta\end{Bmatrix}d\theta dz, \qquad [A3]$$

where $\eta = \mu RL(R/C)^2$, and θ_1 and θ_2 are the film reformation and film rupture boundaries, respectively. The positive (uncavitated) pressure region lies between θ_1 and θ_2. These angular coordinates depend on the position of the journal center within the bearing. Thus, the fluid-film reaction forces are general functions of the journal center displacements and velocities, i.e.,

$$\begin{Bmatrix}F_\varepsilon(e,\phi,\dot{e},\dot{\phi})\\F_\phi(e,\phi,\dot{e},\dot{\phi})\end{Bmatrix} = \eta\omega(1-2\phi')\begin{Bmatrix}\tilde{F}_\varepsilon(\varepsilon,\phi,\varepsilon',\phi')\\\tilde{F}_\phi(\varepsilon,\phi,\varepsilon',\phi')\end{Bmatrix}, \qquad [A4]$$

where $e = C\varepsilon$, and

$$\begin{Bmatrix}\tilde{F}_\varepsilon\\\tilde{F}_\phi\end{Bmatrix} = \int_{-1/2}^{1/2}\int_{\theta_1}^{\theta_2}\tilde{p}\begin{Bmatrix}\cos\theta\\\sin\theta\end{Bmatrix}d\theta d\tilde{z}.$$

The assumption of small amplitude motions about an equilibrium position allows expressing the bearing reaction forces as a Taylor series expansion around the static journal position (ε_0, ϕ_0), i.e.,

$$\begin{aligned}\begin{Bmatrix}f_\varepsilon\\f_\phi\end{Bmatrix} &= \begin{Bmatrix}F_\varepsilon-F_{\varepsilon0}\\F_\phi-F_{\phi0}\end{Bmatrix}\\ &= \left[\left(\Delta e\frac{\partial}{\partial e}+\Delta\phi\frac{\partial}{\partial\phi}+\dot{e}\frac{\partial}{\partial\dot{e}}+\dot{\phi}\frac{\partial}{\partial\dot{\phi}}\right)\begin{Bmatrix}F_\varepsilon\\F_\phi\end{Bmatrix}\right]_{(e=e_0,\phi=\phi_0,\dot{e}=\dot{\phi}=0)}\\ &= \left[\left(\Delta\varepsilon\frac{\partial}{\partial\varepsilon}+\Delta\phi\frac{\partial}{\partial\phi}+\dot{\varepsilon}\frac{\partial}{\partial\dot{\varepsilon}}+\dot{\phi}\frac{\partial}{\partial\dot{\phi}}\right)\begin{Bmatrix}F_\varepsilon\\F_\phi\end{Bmatrix}\right]_{(\varepsilon=\varepsilon_0,\phi=\phi_0,\dot{\varepsilon}=\dot{\phi}=0)}\\ &= -\begin{bmatrix}a_{\varepsilon\varepsilon}&a_{\varepsilon\phi}\\a_{\phi\varepsilon}&a_{\phi\phi}\end{bmatrix}\begin{Bmatrix}C\Delta\varepsilon\\C\varepsilon_0\Delta\phi\end{Bmatrix}-\begin{bmatrix}b_{\varepsilon\varepsilon}&b_{\varepsilon\phi}\\b_{\phi\varepsilon}&b_{\phi\phi}\end{bmatrix}\begin{Bmatrix}C\dot{\varepsilon}\\C\varepsilon_0\dot{\phi}\end{Bmatrix}\end{aligned} \qquad [A5]$$

where

$$a_{\varepsilon\varepsilon} = -\left(\frac{\partial F_\varepsilon}{\partial\varepsilon}\right)_0, b_{\varepsilon\varepsilon} = -\left(\frac{\partial F_\varepsilon}{\partial\dot{\varepsilon}}\right)_0, \ ...$$

are the fluid-film bearing stiffness and damping, respectively. Note that $(C\Delta\varepsilon, C\varepsilon_0\Delta\phi)$ are the radial and tangential displacements of journal center in the (ε,ϕ) coordinate system, and $(C\dot{\varepsilon}, C\varepsilon_0\dot{\phi})$ are the radial and tangential velocities, respectively.

According to Eq. [A4], we can write

$$\begin{Bmatrix}f_\varepsilon\\f_\phi\end{Bmatrix} = \begin{Bmatrix}F_\varepsilon-F_{\varepsilon0}\\F_\phi-F_{\phi0}\end{Bmatrix} = \eta\omega\Bigg[(1-2\phi')\left(\Delta\varepsilon\frac{\partial}{\partial\varepsilon}+\Delta\phi\frac{\partial}{\partial\phi}+\varepsilon'\frac{\partial}{\partial\varepsilon'}+\phi'\frac{\partial}{\partial\phi'}\right)\begin{Bmatrix}\tilde{F}_\varepsilon\\\tilde{F}_\phi\end{Bmatrix}\Bigg]_{(\varepsilon=\varepsilon_0,\phi=\phi_0,\varepsilon'=\phi'=0)} - 2\eta\omega\phi'\begin{Bmatrix}\tilde{F}_\varepsilon\\\tilde{F}_\phi\end{Bmatrix}_{(\varepsilon=\varepsilon_0,\phi=\phi_0,\varepsilon'=\phi'=0)} \qquad [A6]$$

It is assumed that the perturbed pressure field due to small amplitude journal motions about the equilibrium position (ε_0, ϕ_0) does not affect θ_1 andθ_2 delimiting the active film region. So, the normalized Reynolds equation [A2] is quite linear. In this situation, the hydrodynamic forces do not depend on the angular velocity ϕ', i.e.,

$$\left(\frac{\partial \tilde{F}_\varepsilon}{\partial \phi'}\right)_{\varepsilon'=0} = \left(\frac{\partial \tilde{F}_\phi}{\partial \phi'}\right)_{\varepsilon'=0} = 0,$$

and Eq. [A6] becomes:

$$\left\{\begin{matrix} f_\varepsilon \\ f_\phi \end{matrix}\right\} = \eta\omega \left[\left(\Delta\varepsilon \frac{\partial}{\partial \varepsilon} + \Delta\phi \frac{\partial}{\partial \phi} + \varepsilon' \frac{\partial}{\partial \varepsilon'}\right) \left\{\begin{matrix} \tilde{F}_\varepsilon \\ \tilde{F}_\phi \end{matrix}\right\}\right]_{(\varepsilon=\varepsilon_0, \phi=\phi_0, \varepsilon'=\phi'=0)}$$
$$- 2\eta\omega\phi' \left\{\begin{matrix} \tilde{F}_\varepsilon \\ \tilde{F}_\phi \end{matrix}\right\}_{(\varepsilon=\varepsilon_0, \phi=\phi_0, \varepsilon'=\phi'=0)} \quad [A7]$$

Note that

$$\left\{\begin{matrix} \tilde{F}_\varepsilon \\ \tilde{F}_\phi \end{matrix}\right\}_{(\varepsilon=\varepsilon_0, \phi=\phi_0, \varepsilon'=\phi'=0)} = \left\{\begin{matrix} \tilde{F}_{\varepsilon 0} \\ \tilde{F}_{\phi 0} \end{matrix}\right\} = \left\{\begin{matrix} -W_0 \cos\phi_0 \\ W_0 \sin\phi_0 \end{matrix}\right\},$$

which is the equilibrium equation of the journal, W_0 being the applied static load in the X direction (e.g., the weight of rotor per bearing).

According to Eq. [A5] and Eq. [A7], the stiffness and dynamic coefficients can be expressed as

$$a_{\varepsilon\varepsilon} = -\frac{\eta\omega}{C}\left(\frac{\partial \tilde{F}_\varepsilon}{\partial \varepsilon}\right)_0; a_{\varepsilon\phi} = -\frac{\eta\omega}{C\varepsilon_0}\left(\frac{\partial \tilde{F}_\varepsilon}{\partial \phi}\right)_0;$$
$$a_{\phi\varepsilon} = -\frac{\eta\omega}{C}\left(\frac{\partial \tilde{F}_\phi}{\partial \varepsilon}\right)_0; a_{\phi\phi} = -\frac{\eta\omega}{C\varepsilon_0}\left(\frac{\partial \tilde{F}_\phi}{\partial \phi}\right)_0; \quad [A8]$$
$$b_{\varepsilon\varepsilon} = -\frac{\eta}{C}\left(\frac{\partial \tilde{F}_\varepsilon}{\partial \varepsilon'}\right)_0; b_{\varepsilon\phi} = \frac{2\eta}{C\varepsilon_0}\tilde{F}_{\varepsilon 0}; b_{\phi\varepsilon} = -\frac{\eta}{C}\left(\frac{\partial \tilde{F}_\phi}{\partial \varepsilon'}\right)_0;$$
$$b_{\phi\phi} = \frac{2\eta}{C\varepsilon_0}\tilde{F}_{\phi 0}. \quad [A9]$$

The dimensionless dynamic coefficients can be expressed according to the definition

$$A_{ij} = a_{ij}\frac{C}{W_0}, \text{ and } B_{ij} = b_{ij}\frac{C\omega}{W_0},$$

where $(i, j) = (\varepsilon, \phi)$,
or

$$\begin{bmatrix} A_{\varepsilon\varepsilon} & A_{\varepsilon\phi} \\ A_{\phi\varepsilon} & A_{\phi\phi} \end{bmatrix} = -\pi S \begin{bmatrix} \left(\frac{\partial \tilde{F}_\varepsilon}{\partial \varepsilon}\right)_0 & \left(\frac{\partial \tilde{F}_\varepsilon}{\varepsilon_0 \partial \phi}\right)_0 \\ \left(\frac{\partial \tilde{F}_\phi}{\partial \varepsilon}\right)_0 & \left(\frac{\partial \tilde{F}_\phi}{\varepsilon_0 \partial \phi}\right)_0 \end{bmatrix};$$

$$\begin{bmatrix} B_{\varepsilon\varepsilon} & B_{\varepsilon\phi} \\ B_{\phi\varepsilon} & B_{\phi\phi} \end{bmatrix} = -\begin{bmatrix} \pi S\left(\frac{\partial \tilde{F}_\varepsilon}{\partial \varepsilon'}\right)_0 & \frac{2\cos\phi_0}{\varepsilon_0} \\ \pi S\left(\frac{\partial \tilde{F}_\phi}{\partial \varepsilon'}\right)_0 & \frac{-2\sin\phi_0}{\varepsilon_0} \end{bmatrix}, \quad [A10]$$

where

$$S = \frac{\mu\omega RL\left(R/C\right)^2}{\pi W_0} = \frac{1}{\pi \bar{W}_0}$$

is the dimensionless Sommerfeld number.

In the following, we will demonstrate that the cross-damping coefficients of hydrodynamic journal bearings with rigid-liner are always identical. According to Eq. [A10], we have

$$\begin{cases} B_{\phi\varepsilon} = -\pi S\left(\frac{\partial \tilde{F}_\phi}{\partial \varepsilon'}\right)_0 \\ B_{\varepsilon\phi} = -\frac{2\cos\phi_0}{\varepsilon_0} \end{cases} \quad [A11]$$

where

$$\tilde{F}_\phi = \int_{-1/2}^{1/2}\int_{\theta_1}^{\theta_2} \tilde{p}\,(\theta, \tilde{z}, \varepsilon, \varepsilon')\sin\theta d\theta d\tilde{z} \quad [A12]$$

and

$$\frac{\partial \tilde{F}_\phi}{\partial \varepsilon'} = \int_{-1/2}^{1/2}\int_{\theta_1}^{\theta_2} \frac{\partial \tilde{p}}{\partial \varepsilon'}\sin\theta d\theta d\tilde{z}. \quad [A13]$$

Taking into account the linearity of the Reynolds equation Eq. [A2] with respect to ε', we can write

$\tilde{p} = \tilde{p}_0 + \varepsilon'\tilde{p}_1$,where $\tilde{p}_0$ represents the nondimensional steady-state pressure field, and $\tilde{p}_1$ represents the dynamic pressure field added to $\tilde{p}_0$ for $\varepsilon' = 1$. Equation [A13] becomes

$$\frac{\partial \tilde{F}_\phi}{\partial \varepsilon'} = \int_{-1/2}^{1/2}\int_{\theta_1}^{\theta_2} \tilde{p}_1\sin\theta d\theta d\tilde{z} \quad [A14]$$

Note that $\tilde{p}_1$ and $\tilde{p}_0$ are the solutions of the following equations:

$$\Re\left(\tilde{p}_1\right) = \cos\theta, \quad [A15]$$

$$\Re\left(\tilde{p}_0\right) = \frac{1}{2}\frac{\partial \tilde{h}}{\partial \theta} = -\frac{\varepsilon_0\sin\theta}{2}. \quad [A16]$$

From Eq. [A16], we can obtain

$$\sin\theta = -\frac{2}{\varepsilon_0}\Re\left(\tilde{p}_0\right). \quad [A17]$$

Substituting Eq. [A17] into Eq. [A14], we get

$$\frac{\partial \tilde{F}_\phi}{\partial \varepsilon'} = -\frac{2}{\varepsilon_0}\int_{-1/2}^{1/2}\int_{\theta_1}^{\theta_2} \tilde{p}_1\Re\left(\tilde{p}_0\right)d\theta d\tilde{z}. \quad [A18]$$

Integrating by parts, we obtain

$$\frac{\partial \tilde{F}_\phi}{\partial \varepsilon'} = +\frac{2}{\varepsilon_0}\int_{-1/2}^{1/2}\int_{\theta_1}^{\theta_2}\left(\frac{\tilde{h}^3}{12}\frac{\partial \tilde{p}_0}{\partial \theta}\frac{\partial \tilde{p}_1}{\partial \theta} + (R/L)^2\frac{\tilde{h}^3}{12}\frac{\partial \tilde{p}_0}{\partial \tilde{z}}\frac{\partial \tilde{p}_1}{\partial \tilde{z}}\right)d\theta d\tilde{z}. \quad [A19]$$

A new integration by parts gives

$$\frac{\partial \tilde{F}_\phi}{\partial \varepsilon'} = -\frac{2}{\varepsilon_0}\int_{-1/2}^{1/2}\int_{\theta_1}^{\theta_2} \tilde{p}_0\Re\left(\tilde{p}_1\right)d\theta d\tilde{z}. \quad [A20]$$

According to Eq. [A15], Eq. [A20] takes the following form:

$$\left(\frac{\partial \tilde{F}_\phi}{\partial \varepsilon'}\right)_0 = -\frac{2}{\varepsilon_0}\int_{-1/2}^{1/2}\int_{\theta_1}^{\theta_2} \tilde{p}_0\cos\theta d\theta d\tilde{z} = -\frac{2\tilde{F}_{\varepsilon 0}}{\varepsilon_0}.$$

Consequently,

$$B_{\phi\varepsilon} = -\pi S\left(\frac{\partial \tilde{F}_\phi}{\partial \varepsilon'}\right)_0 = \frac{2\pi S\tilde{F}_{\varepsilon 0}}{\varepsilon_0}.$$

Since

$$\tilde{F}_{\varepsilon 0} = -\bar{W}_0\cos\phi_0, \text{ and} S = \frac{1}{\pi\bar{W}_0}.$$

we get

$$B_{\phi\varepsilon} = -\frac{2\cos\phi_0}{\varepsilon_0}.$$

Thus, the cross-damping coefficients are quite identical: ($B_{\phi\varepsilon} = B_{\varepsilon\phi}$).

For the plain journal bearings (without axial groove), the expression and the calculation of dynamic coefficients are simplified because the pressure field does not depend on the attitude angle due to the circumferential symmetry. For this particular case, and according to the relations stated above, we have

$$A_{\varepsilon\phi} = \frac{\sin\phi_0}{\varepsilon_0}; A_{\phi\phi} = \frac{\cos\phi_0}{\varepsilon_0}; \quad B_{\phi\phi} = 2A_{\varepsilon\phi}; \text{ and } B_{\varepsilon\phi} = -2A_{\phi\phi}. \qquad [A21]$$

It should be noted that the pressure boundary conditions related to the environment and to the flow of lubricant in the clearance space of the journal bearing appreciably modify the values of the dynamic coefficients; some of them vanish or become negative.